4

Physical Layer Techniques

4.1 Introduction

Communication is the transmission of information from a source to one or more destinations. To enable this, communications protocols or communications models are required. The most widely used communications protocol is the transmission control protocol/internet protocol (TCP/IP) model, which has four layers stacked from the bottom to the top as the network interface layer, the internet layer, the transport layer, and the application layer. Another frequently used model is the open systems interconnection (OSI) model, which has seven layers stacked from the bottom to the top as the physical layer, the link layer, the network layer, the transport layer, the session layer, the presentation layer, and the application layer. These two models have certain equivalence in terms of functions. In wireless communications, it is often the physical layer and the link layer in the OSI model, equivalent to the network interface layer in the TCP/IP model, that are of interest. The physical layer performs the transmission and reception of the physical bits, while the link layer provides control functions to enable the efficient operations of transmission and reception. Figure 4.1 shows diagrams of these models. One sees that the physical layer lies at the bottom of the whole system. Any issue in this layer will affect the whole system. Thus, this layer is the most important layer in any communications systems. It will be studied first.

The main purpose of the physical layer is to provide reliable and efficient transmission and reception of the information. Many communications techniques, such as modulation, channel encoding, multiple-input-multiple-output (MIMO) and orthogonal-frequency-division-multiplexing (OFDM), are designed to achieve this purpose. At the core of all these techniques, no matter how the signals are modulated or encoded and no matter which antennas or subcarriers the transmitter uses, the received signals must be detected to recover the transmitted information. Therefore, signal detection is the most important task of the physical layer.

There are many different types of signal detectors, such as coherent detectors, non-coherent detectors, energy detectors, and differential detectors (Kay 1998). They have different performances and can be used for different applications. In applications where performance is of utmost importance, coherent detectors can be used. In these detectors, in order to achieve the best performance, the system state information, such as the channel parameters and the transmitter parameters, is often useful to facilitate the signal detection. Such information can be provided by performing signal estimation

Energy Harvesting Communications: Principles and Theories, First Edition. Yunfei Chen.

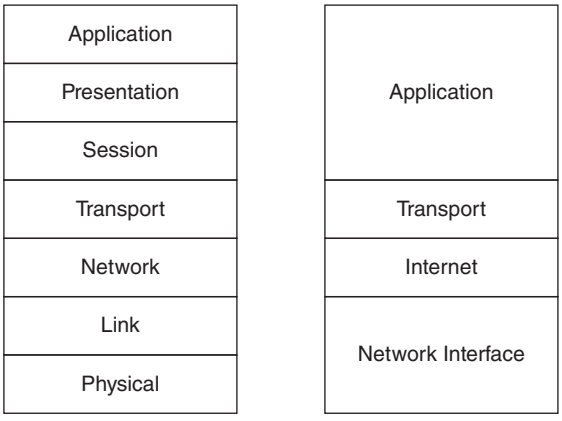

Figure 4.1 Diagrams of (a) OSI and (b) TCP/IP models.

or parameter estimation. Thus, signal estimation is another important part of the physical layer (Kay 1993).

In addition to signal detection and signal estimation, which are mainly conducted at the receiver or the destination, in some cases, the transmitter or the source can also perform pre-distortion or pre-coding for best performance. For example, in conventional communications systems with information only, the transmitter can perform beamforming to achieve diversity gain or Nyquist pulse shaping to avoid inter-symbol interference. Similarly, in energy harvesting communications systems with both information and power, the transmitter can also adopt waveform designs to make the power transfer most efficient.

Next, we will first evaluate the effect of energy harvesting on communications, and then we will study signal detection, channel estimation and waveform design for energy harvesting communications systems. After that, we will have a brief discussion on other important issues and techniques in the physical layer of the energy harvesting communications systems.

4.2 Effect of Energy Harvesting

The main effect of energy harvesting on wireless communications is the dynamic power supply. In this book, the radio frequency (RF) energy harvester will be used as an example to examine this effect. Unlike other energy sources, such as solar/light and mechanical energies, the RF signal can be used for both power transfer and information delivery. It is also relatively easier to control. Thus, it provides a good example of how the energy harvesting capability can be integrated with existing communications techniques to implement energy harvesting communications. To do this, first, we will derive the distribution of the random transmission power in some special cases. The randomness comes from the random channel between the power transmitter and the RF energy harvester in this case. Then, using this random power supply, we will discuss a tradeoff between the transmission delay and the transmission probability, when the harvested energy is accumulated for fixed-power transmission. After that, we will use the random power supply to derive the bit error rate (BER) and the achievable

rate of the wireless system, where BER measures the reliability of the system while the achievable rate measures the capacity of the system, when the harvested energy is used immediately after being harvested for variable-power transmission. Finally, we will discuss some general information theoretic limits for all energy sources, including the RF power.

4.2.1 Distribution of Transmission Power

Chapter 3 considered the general case when different harvesters are adopted to harvest energy from signals over different antennas, frequency bands or time slots with independent but non-identically distributed channels. This generality has led to the complicated expressions for the probability density function of the harvested power. In this subsection, we will only consider the special case when the same harvester is employed to harvest energy over different time slots or when the channels are independent and identically distributed.

More specifically, consider an energy harvesting wireless system. In this system, the base station or the access point are power sources that transfer a certain amount of wireless power to the remote user devices for charging first. The remote devices then use only the harvested energy to transmit their data back to the base station. This could be a wireless sensor network where the access point collects data from sensors in the field or could be a cellular network where mobile users receive power supply from a power beacon. All devices are assumed half-duplex with a single antenna. Each power transfer or data transmission is performed in a time slot of T seconds. In order to harvest enough energy for transmission, the remote device has to harvest energy from K time slots with a total of KT seconds.

Using the above assumptions, one can divide the whole communication process into two stages. In the first stage, the RF power source (base station or access point) transfers RF power to the remote device as

$$y_k = h_k\sqrt{P_s}s_k + n_k \tag{4.1}$$

where $k = 1, 2, \cdots, K$ denote the K time slots over which the remote device harvests energy, h_k is the fading coefficient from the power source to the remote device and is a complex Gaussian random variable with mean s and variance $2\alpha^2$, P_s is the transmission power for power transfer (different from the transmission power for information delivery discussed later), s_k is the energy signal with $s_k = 1$ for simplicity, and n_k is the complex additive white Gaussian noise (AWGN) with mean zero and variance $2\sigma^2$. In this case, $s = 0$ gives the Rayleigh fading channels, and $s \neq 0$ gives the general Rician fading channels. It is easy to derive that the mean of y_k in (4.1) is

$$\mu = s\sqrt{P_s} \tag{4.2}$$

as $s_k = 1$ and the variance of y_k in (4.1) is

$$2\beta^2 = 2\alpha^2 P_s + 2\sigma^2. \tag{4.3}$$

Using (4.1), the total amount of energy harvested over K time slots can be derived as

$$E = \eta \sum_{k=1}^{K} |y_k|^2 T = \eta T \sum_{k=1}^{K} |h_k\sqrt{P_s} + n_k|^2 \tag{4.4}$$

where η is the conversion efficiency of the energy harvester and is the same for all K signals, as the same harvester is used for K times.

In the second stage, the harvested energy in (4.4) is used by the remote device to transmit its data back to the access point. One has the received signal at the access point as

$$r = g\sqrt{P_x}x + n \tag{4.5}$$

where g is the fading coefficient in this channel, P_x is the transmission power for information delivery and it may be different from P_s for power transfer, x is the transmitted symbol, and n is the complex AWGN with mean zero and variance $2\sigma_d^2$. Assume that g is complex Gaussian distributed with mean s_d and variance $2\alpha_d^2$. Using (4.4), the signal transmission power satisfies $P_x \leq P$, where P is the harvested power given by

$$P = \frac{E}{T} = \eta\beta^2 W \tag{4.6}$$

with

$$W = \sum_{k=1}^{K} \left| \frac{h_k\sqrt{P_s} + n_k}{\beta} \right|^2. \tag{4.7}$$

If the remote device has a limited battery capacity, such as a supercapacitor, the energy needs to be used as soon as it is harvested. In this energy usage protocol, $P_x = P$. Since W is a random variable, both P and P_x will randomly change, leading to a variable-power transmission. If the remote device has a large battery capacity, such as a rechargeable battery, the harvested energy can be stored and accumulated until it is needed. In this case, P_x can be a fixed value, leading to a fixed-power transmission. In this case, for conventional communications, the system performance is only affected by the random fading g, while for energy harvesting communications, the system performance is affected by both the random fading g and the random power P caused by the random fading during power transfer.

In the general Rician fading channels, W is a sum of the squares of $2K$ (both real and imaginary parts of y_k) independent Gaussian random variables with non-zero mean and unit variance. Thus, it can be derived as a non-central chi-square random variable with $2K$ degrees of freedoms and non-centrality parameter $\lambda = KP_s\frac{|s|^2}{\beta^2}$ (Proakis 2001). Using this fact and the relationship of $P = \eta\beta^2 W$, one has the probability density function (PDF) and the cumulative distribution function (CDF) of P as

$$f_P(y) = \frac{e^{-\frac{y}{2\eta\beta^2} - \frac{KP_s|s|^2}{2\sigma^2}}}{2\eta\beta^2(\eta KP_s|s|^2)^{\frac{K-1}{2}}} y^{\frac{K-1}{2}} I_{K-1}\left(\sqrt{\frac{KP_s|s|^2 y}{\eta\beta^4}}\right) \tag{4.8}$$

and

$$F_P(y) = 1 - Q_K\left(\sqrt{\frac{KP_s|s|^2}{\beta^2}}, \sqrt{\frac{y}{\eta\beta^2}}\right) \tag{4.9}$$

respectively, where $I_{K-1}(\cdot)$ is the $(K-1)$th order modified Bessel function of the first kind Gradshteyn and Ryzhik (2000, eq. (8.406.1)) and $Q_K(\cdot,\cdot)$ is the Kth order Marcum Q function Proakis (2001, eq. (2.1–122)).

In the special case of Rayleigh fading channels, $s = 0$. Then, it can be derived that W is a central chi-square random variable with $2K$ degrees of freedom, equivalent to a Gamma random variable with shape parameter K and scale parameter 2. Again, since $P = \eta\beta^2 W$, the PDF and CDF of P are derived, respectively, as

$$f_P(y) = \frac{y^{K-1}}{(2\eta\beta^2)^K \Gamma(K)} e^{-\frac{y}{2\eta\beta^2}} \tag{4.10}$$

and

$$F_P(y) = \frac{\gamma(K, \frac{y}{2\eta\beta^2})}{\Gamma(K)} \tag{4.11}$$

where $\Gamma(\cdot)$ is the Gamma function Gradshteyn and Ryzhik (2000, eq. (8.310.1)) and $\gamma(\cdot, \cdot)$ is the incomplete Gamma function Gradshteyn and Ryzhik (2000, eq. (8.350.1)). These distributions will be used in the following subsections to examine the effect of energy harvesting on wireless performances. In contrast, for a conventional wireless communications system, P and P_x are fixed.

4.2.2 Transmission Delay and Probability

Consider the fixed-power transmission using a rechargeable battery first. In this case, the remote device harvests energy from K time slots until the harvested power P is larger than or equal to the required fixed transmission power P_x. Then, the remote device uses the harvested energy to transmit its data to the base station in the next time slot for T seconds. There is a tradeoff here. If the remote device harvests the energy for a longer time, there will be a higher probability that it has enough energy for information transmission or a larger transmission probability. On the other hand, a longer harvesting time will cause a larger transmission delay and thus reduces the system throughput, as this time could have been used for information transmission. An optimum value of K exists, and will be studied next.

To study this tradeoff, define the transmission probability as

$$P_T = Pr\{P \geq P_x\} = Pr\{\Lambda \geq \Lambda_x\} \tag{4.12}$$

where $\Lambda = \frac{P}{2\sigma_d^2}$ and $\Lambda_x = \frac{P_x}{2\sigma_d^2}$. The first equation in (4.12) makes sure that the harvested power is larger than or equal to the required power in order to transmit the information. Such a fixed value of P_x can be required to guarantee certain quality of service (QoS). The second equation translates the power limitation into the signal-to-noise ratio (SNR) limitation, where the transmission SNR must be larger than or equal to the required SNR. Since the noise power $2\sigma_d^2$ is a constant, these two limitations are equivalent.

On the other hand, the transmission delay is KT seconds, caused by energy harvesting. Since the actual time for information transmission is T seconds, the effective throughput is $\frac{1}{K+1}$. This effective throughput is only possible when the remote device actually performs transmission. Thus, the average throughput can be defined as

$$C = \frac{1}{K+1} P_T. \tag{4.13}$$

This value will be our performance measure used to consider the tradeoff between the transmission delay and the transmission probability. Its calculation boils down to the calculation of P_T, which requires the CDF of P.

Using (4.9), the average throughput in Rician fading channels can be calculated as

$$C = \frac{1}{K+1} Q_K \left(\sqrt{\frac{KP_s|s|^2}{\beta^2}}, \sqrt{\frac{2\sigma_d^2 \Lambda_x}{\eta \beta^2}} \right) \tag{4.14}$$

and using (4.11), the average throughput in Rayleigh fading channels becomes

$$C = \frac{1}{K+1} \left[1 - \frac{\gamma\left(K, \frac{2\sigma_d^2 \Lambda_x}{2\eta\beta^2}\right)}{\Gamma(K)} \right]. \tag{4.15}$$

One notes that (4.15) can also be obtained from (4.14) by setting $s = 0$ and using the relationship between the Marcum Q function and the Gamma function. One can see from these equations that C decreases when $K + 1$ increases but increases when K in the Gamma function or the Marcum Q function increases. Thus, an optimum K may exist. Note again that this is the case when the remote device can use a large rechargeable battery for storage so that fixed-power transmission is possible to guarantee the QoS. This is not possible for supercapacitors that have very limited storage.

Next, some numerical examples will be given to show the effect of energy harvesting on this tradeoff. In these examples, we examine the values of Λ_x from 0 to 20 dB with a step size of 2 dB and the values of K from 1 to 20 with a step size of 1 for the average throughput C. We set $\eta = 0.5$, which corresponds to a 50% efficiency for the RF energy harvester. We also define $\omega = \frac{\Omega P_s}{2\sigma^2}$ as the average SNR in the power transfer channel, where $\Omega = |s|^2 + 2\alpha^2$. This value indicates the quality of the random channel from the power source to the remote device. Figures 4.2–4.4 show the relationship between C and K under different conditions. For Rayleigh fading channels, $s = 0$.

From Figure 4.2, first, one can see that, for $\Lambda_x = 2$ dB, C monotonically decreases with K, while for other values of Λ_x, C first increases then decreases with K. This

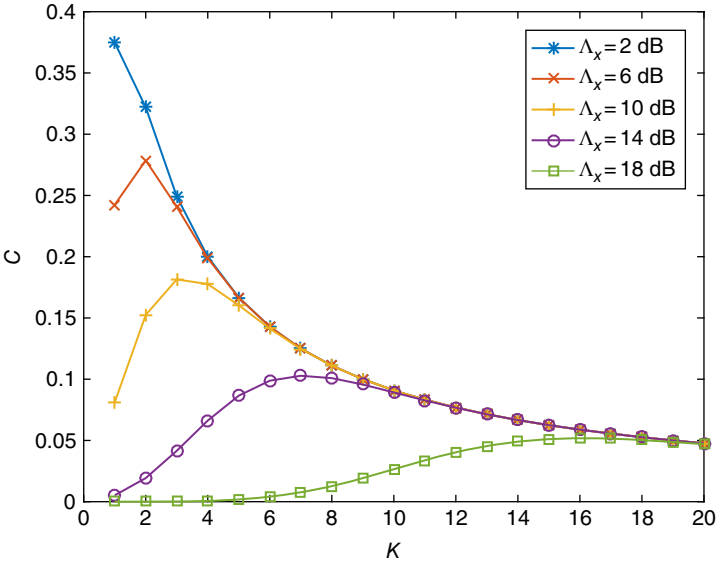

Figure 4.2 C versus K in Rayleigh fading channels when $\omega = 10$ dB.

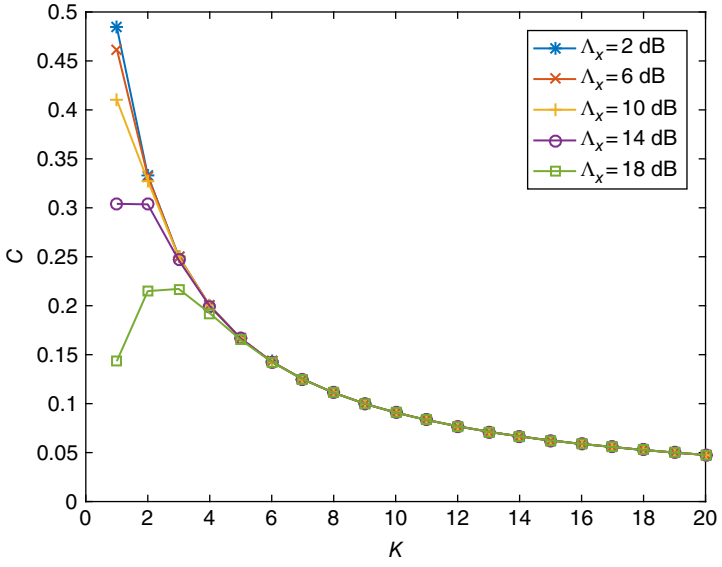

Figure 4.3 C versus K in Rayleigh fading channels when $\omega = 20$ dB.

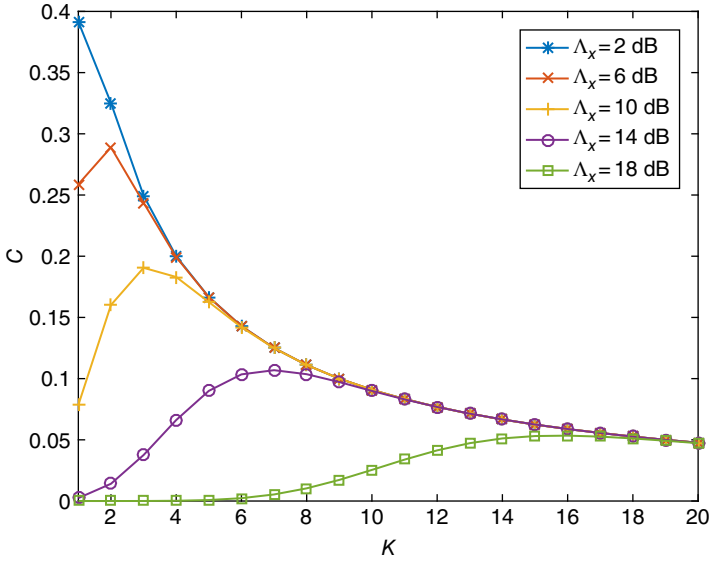

Figure 4.4 C versus K in Rician fading channels when $\omega = 10$ dB and $\frac{|s|^2}{2\alpha^2} = 1$.

implies that the optimum value of K exists, as expected. Based on this observation, in order to achieve a balance between transmission probability and transmission delay, for $\Lambda_x = 2$ dB, one should choose $K = 1$, for $\Lambda_x = 6$ dB, one should choose $K = 2$, and so on. Thus, these curves give very useful guidance on how the harvesting time should be chosen. Secondly, the optimum value of C in general decreases with Λ_x, implying that, if one requires a higher transmission power or data rate for information

transmission, it will lead to an overall larger delay or smaller throughput. Thirdly, when K is large, the values of C for different values of Λ_x tend to overlap with each other. This can be explained using the results for Rayleigh fading channels. Using an equation in Gradshteyn and Ryzhik (2000, eq. (8.352.1)), $C = \frac{1}{K+1} e^{-\frac{2\sigma_d^2 \Lambda_x}{2\eta\beta^2}} \sum_{m=0}^{K-1} \frac{(\frac{2\sigma_d^2 \Lambda_x}{2\eta\beta^2})^m}{m!}$ in (4.15). When $K \to \infty$, $\sum_{m=0}^{K-1} \frac{(\frac{2\sigma_d^2 \Lambda_x}{2\eta\beta^2})^m}{m!} \to e^{\frac{2\sigma_d^2 \Lambda_x}{2\eta\beta^2}}$ according to the Taylor series expansion of exponential functions. Thus, $C \to \frac{1}{K+1}$, independent of Λ_x.

Also, comparing Figure 4.3 with Figure 4.2, one can see that, when ω increases because of either an increase in $2\alpha^2$ and P_s or a decrease in $2\sigma^2$, C increases in general. In this case, the optimum value of K decreases, as expected, as less time slots will be required if less power is lost in a better channel from the power source to the remote device. Finally, comparing Figure 4.4 with Figure 4.2, one can see that, when the channel condition changes from Rayleigh to Rician or when $|s|^2$ increases, C increases slightly.

Figures 4.5 and 4.6 show C versus Λ_x to examine the effect of Λ_x on the system performance more clearly.

From Figure 4.5, one sees that C does not change with Λ_x and then gradually decreases to zero, when Λ_x increases, in most cases considered. This suggests that Λ_x cannot be chosen too large in the design. Particularly, in Figure 4.5, Λ_x should be smaller than 8 dB for $K = 4$, 12 dB for $K = 6$, and so on.

Beyond these threshold values, the transmission delay will be too large to be compensated by the harvested energy in the average throughput. Note that C generally increases when K decreases due to smaller delay but there is a range determined by Λ_x. For example, when Λ_x is less than 12 dB, $K = 4$ has a larger C than $K = 6$, but when Λ_x is larger than 12 dB, C for $K = 4$ decreases faster so that it is disadvantageous to use a smaller K. These threshold values change with K. Finally, comparing Figure 4.6 with

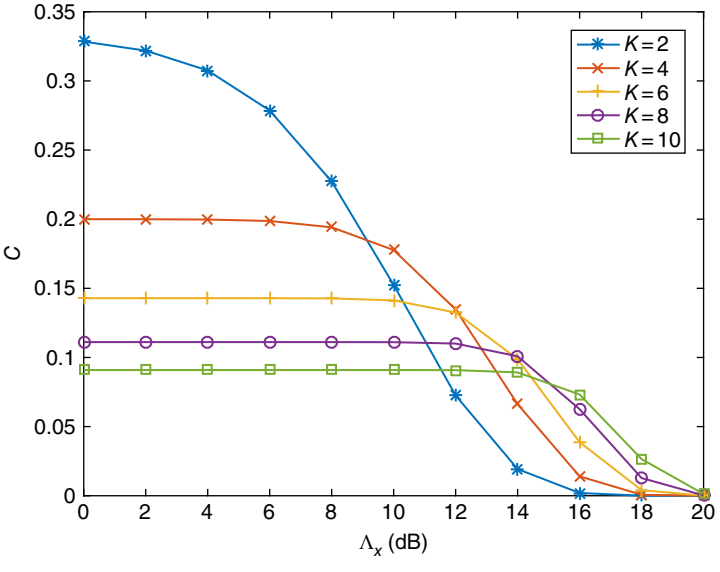

Figure 4.5 C versus Λ_x in Rayleigh fading channels when $\omega = 10$ dB.

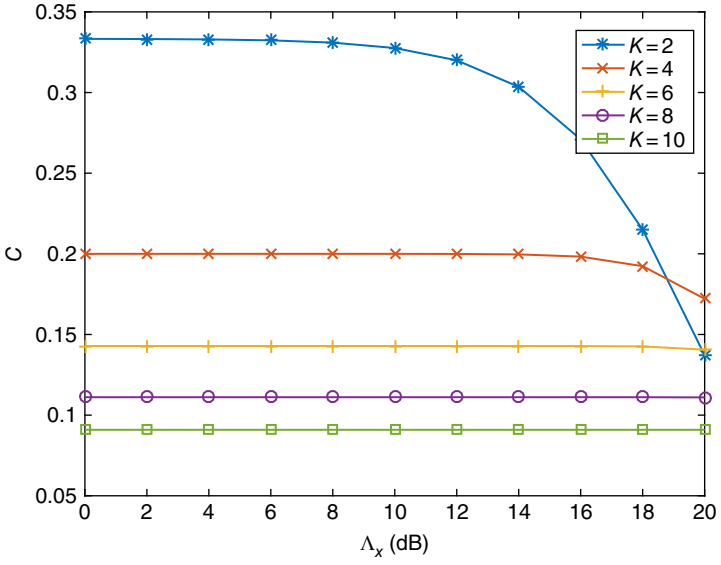

Figure 4.6 C versus Λ_x in Rayleigh fading channels when $\omega = 20$ dB.

Figure 4.5, the range where C remains constant increases when ω increases, implying that there will be more choices or more flexibility when the channel conditions are better.

From the above results, for energy harvesting communications, the choices of harvesting time and QoS are quite important. For the best tradeoff between transmission probability and transmission delay, the optimum number of harvesting time slots should be used within a certain range of QoS. For conventional communications, there is no delay caused by energy harvesting so the value of C is always 1, which is larger than that for energy harvesting communications. Thus, the randomness in power supply causes performance degradation.

4.2.3 Bit Error Rate

In the previous subsection, the fixed-power transmission scheme was studied. In this subsection and the next subsection, the variable-power transmission scheme is considered. In this scheme, the remote device uses a supercapacitor with a limited capacity such that the harvested energy is used as soon as possible. One practical motivation for this scheme is that most batteries suffer from leakage. The longer the energy is stored, the more leakage it will incur. Also, to have fixed-power transmission, as in the previous subsection, power management will be required. This may complicate the energy harvester design and thus may not be desirable or necessary in simple low-power applications.

The error rate or the probability of error measures the reliability of a wireless system. It will be studied in this subsection. The achievable rate measures the capacity of a wireless channel. It will be examined in the next subsection. Using (4.5), the overall SNR of the received data signal can be derived as

$$\epsilon = \frac{|g|^2}{2\sigma_d^2} P_x = \gamma P_x \tag{4.16}$$

where $\gamma = \frac{|g|^2}{2\sigma_d^2}$ is the SNR from fading. Since the energy is used as soon as it is harvested, one has $P_x = P$ so that

$$\epsilon = \gamma P. \tag{4.17}$$

As mentioned before, for conventional communications, the only randomness in the received SNR comes from the fading coefficient g, while for energy harvesting communications, the randomness in the received SNR comes from both the fading coefficient g and the transmission power P. Next, we use binary signaling as an example to analyze the BER.

From (4.5), it can be shown using results in Simon and Alouini (2005) that binary signals with coherent detection have BERs of

$$P_e(\epsilon) = Q(\sqrt{2u\epsilon}) \tag{4.18}$$

where $u = 1$ for binary phase shift keying (BPSK), $u = \frac{1}{2}$ for binary frequency shift keying (BFSK), $Q(\cdot)$ is the Gaussian Q function Proakis (2001, eq. (2.1–97)), and ϵ is given in (4.17). Also, from Simon and Alouini (2005), for binary signals with non-coherent detection, their BERs are given by

$$P_e(\epsilon) = \frac{1}{2}e^{-u\epsilon} \tag{4.19}$$

where $u = 1$ for differential phase shift keying (DPSK) and $u = \frac{1}{2}$ for BFSK. These expressions are conditional BERs, conditioned on the SNR ϵ. Next, we need to find the distribution of ϵ to calculate the unconditional BERs.

Consider the simpler Rayleigh fading channels first. In this case, it can be shown that the PDF of γ is given by

$$f_\gamma(x) = \frac{1}{\bar{\gamma}}e^{-\frac{x}{\bar{\gamma}}} \tag{4.20}$$

where $\bar{\gamma} = \frac{2\alpha_d^2}{2\sigma_d^2}$ is the average SNR of the channel. Using (4.20) and (4.10), the PDF of ϵ is calculated as

$$f_\epsilon(z) = \frac{2z^{\frac{K-1}{2}}}{(2\eta\beta^2\bar{\gamma})^{\frac{K+1}{2}}\Gamma(K)}K_{K-1}\left(\sqrt{\frac{2z}{\eta\beta^2\bar{\gamma}}}\right) \tag{4.21}$$

where $K_{K-1}(\cdot)$ is the $(K-1)$th order modified Bessel function of the second kind Gradshteyn and Ryzhik (2000, eq. (8.407.1)). Similarly, the CDF of ϵ can be calculated as

$$F_\epsilon(z) = 1 - \frac{z^{\frac{K}{2}}}{(2\eta\beta^2\bar{\gamma})^{\frac{K}{2}}\Gamma(K)}K_K\left(\sqrt{\frac{2z}{\eta\beta^2\bar{\gamma}}}\right). \tag{4.22}$$

Using (4.19) and (4.21), the average BER for binary signaling with non-coherent detection is obtained as

$$\bar{P}_e = \frac{e^{\frac{1}{4u\eta\beta^2\bar{\gamma}}}}{2(2u\eta\beta^2\bar{\gamma})^{\frac{K}{2}}}W_{-\frac{K}{2},\frac{K-1}{2}}\left(\frac{1}{2u\eta\beta^2\bar{\gamma}}\right) \tag{4.23}$$

where an equation in Gradshteyn and Ryzhik (2000, eq. (6.631.3)) has been used and $W(\cdot,\cdot)$ is the Whittaker function Gradshteyn and Ryzhik (2000, eq. (9.220.4)). Also,

using (4.18) and (4.22), the average BER of binary signaling with coherent detection is derived as

$$\bar{P}_e = \frac{1}{2} - \frac{\sqrt{u\eta\beta^2\bar{\gamma}/2}\Gamma(K+0.5)}{2(2u\eta\beta^2\bar{\gamma})^{\frac{K}{2}}\Gamma(K)} e^{\frac{1}{4u\eta\beta^2\bar{\gamma}}} W_{-\frac{K}{2},\frac{K}{2}}\left(\frac{1}{2u\eta\beta^2\bar{\gamma}}\right). \tag{4.24}$$

These expressions can be used to examine the choice of the number of time slots. Next, we study the more complicated Rician fading channels.

In Rician fading channels, the PDF of γ can be derived as

$$f_\gamma(x) = \frac{1}{\bar{\gamma}} e^{-\frac{|s_d|^2}{2\alpha_d^2} - \frac{x}{\bar{\gamma}}} I_0\left(\sqrt{\frac{2x|s_d|^2}{\bar{\gamma}\alpha_d^2}}\right). \tag{4.25}$$

Then, using (4.25) and (4.8), the PDF of ϵ is

$$f_\epsilon(z) = \frac{e^{-\frac{KP_s|s|^2}{2\beta^2} - \frac{|s_d|^2}{2\alpha_d^2}}}{2\eta\beta^2\bar{\gamma}(\eta KP_s|s|^2)^{\frac{K-1}{2}}} \int_0^\infty x^{\frac{K-3}{2}} e^{-\frac{x^2}{2\eta\beta^2} - \frac{z}{x\bar{\gamma}}} I_{K-1}\left(\sqrt{\frac{KP_s|s|^2x}{\eta\beta^4}}\right) I_0\left(\sqrt{\frac{2z|s_d|^2}{\bar{\gamma}\alpha_d^2 x}}\right) dx. \tag{4.26}$$

The CDF of ϵ can be derived similarly as

$$F_\epsilon(z) = 1 - \frac{e^{-\frac{KP_s|s|^2}{2\beta^2}}}{2\eta\beta^2(\eta KP_s|s|^2)^{\frac{K-1}{2}}} \int_0^\infty x^{\frac{K-1}{2}} e^{-\frac{x}{2\eta\beta^2}} I_{K-1}\left(\sqrt{\frac{KP_s|s|^2x}{\eta\beta^4}}\right) Q_1\left(\frac{|s_d|}{\alpha_d}, \sqrt{\frac{2z}{\bar{\gamma}x}}\right) dx. \tag{4.27}$$

Thus, (4.26) can be used to calculate the average BER for non-coherent detection as

$$\bar{P}_e = \frac{e^{-\frac{KP_s|s|^2}{2\beta^2} - \frac{|s_d|^2}{2\alpha_d^2}}}{4\eta\beta^2(\eta KP_s|s|^2)^{\frac{K-1}{2}}} \int_0^\infty \frac{x^{\frac{K-1}{2}}}{\sqrt{\frac{|s_d|^2}{2\alpha_d^2}(1+\bar{\gamma}ux)}} e^{-\frac{x}{2\eta\beta^2} + \frac{|s_d|^2/(2\alpha_d^2)}{2(1+\bar{\gamma}ux)}} I_{K-1}\left(\sqrt{\frac{KP_s|s|^2x}{\eta\beta^4}}\right) M_{-\frac{1}{2},0}\left(\frac{|s_d|^2/(2\alpha_d^2)}{1+\bar{\gamma}ux}\right) dx \tag{4.28}$$

where an equation in Gradshteyn and Ryzhik (2000, eq. (6.614.3)) has been used and $M(\cdot,\cdot)$ is another type of Whittaker function defined by Gradshteyn and Ryzhik (2000, eq. (9.220.2)). Also, (4.27) can be used with integration by parts to give the average BER for coherent detection as

$$\bar{P}_e = \frac{e^{-\frac{KP_s|s|^2}{2\beta^2} - \frac{|s_d|^2}{2\alpha_d^2}}}{4\eta\beta^2(\eta KP_s|s|^2)^{\frac{K-1}{2}}} \int_0^\infty x^{\frac{K-1}{2}} e^{-\frac{x}{2\eta\beta^2}} \sqrt{\frac{\bar{\gamma}ux}{\bar{\gamma}ux+1}} I_{K-1}\left(\sqrt{\frac{KP_s|s|^2x}{\eta\beta^4}}\right) \left[\Phi_1\left(0.5,1,1;\frac{1}{\bar{\gamma}ux+1};\frac{|s_d|^2/(2\alpha_d^2)}{\bar{\gamma}ux+1}\right) - {}_1F_1\left(0.5;1;\frac{|s_d|^2/(2\alpha_d^2)}{\bar{\gamma}ux+1}\right)\right] dx. \tag{4.29}$$

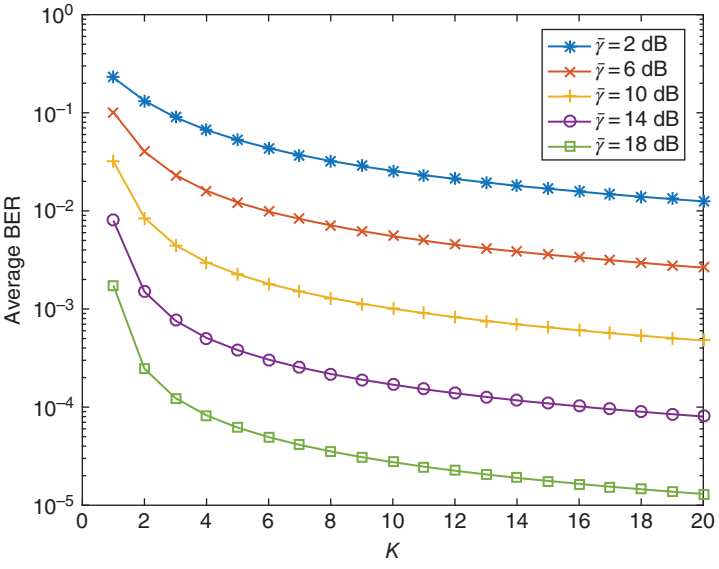

Figure 4.7 Average BER versus K in Rayleigh fading channels.

where an elegant result in Sofotasios et al. (2015) has been used, $\Phi_1(\cdot,\cdot,\cdot;\cdot;\cdot)$ and ${}_1F_1(\cdot;\cdot;\cdot)$ are the hypergeometric functions (Sofotasios et al. 2015).

Figures 4.7 and 4.8 give the average BER. For simplicity, we only consider coherent detection of BFSK in the Rayleigh fading channels and assume that $s_d = s = 0$, $\alpha_d^2 = \alpha^2$, and $\sigma_d^2 = \sigma^2$. Thus, $\omega = \bar{\gamma}$ in this case. From Figure 4.7, one can see that the average BER first decreases quickly with K but then is only marginally reduced when K keeps increasing. Since a larger value of K requires a larger capacity of the supercapacitor and also possibly causes more leakage, it is desirable to use a small value of K, less than $K = 3$ in most cases considered. This is also confirmed by Figure 4.8, where the average BER also decreases with K but the performance gain at small values of K is larger than that at large values of K. The BER performance reaches a lower limit as K keeps increasing.

Figure 4.9 compares the BER performances of coherent BFSK in conventional communications and energy harvesting communications when $K = 1$. For the conventional communications in the figure, the SNR is given by $\epsilon = 2K\eta\beta^2\gamma$, where $2K\eta\beta^2$ is the average of P in energy harvesting communications so that both cases have the same average overall SNR for a fair comparison. One can see that the BER performance is degraded by energy harvesting, due to the random variation in power supply, as expected.

One sees from these figures that, in general, the effect of energy harvesting on the BER diminishes quickly when the harvesting time increases. Taking this observation and the practical limitation on the supercapacitor into account, the number of time slots for energy harvesting should be chosen as small as possible. Note also that the above results effectively evaluate the average BER averaged over ϵ, which is a product of γ and P. Similar results have also been obtained in conventional communications without energy harvesting. For example, in dual-hop wireless relaying, the BER can be averaged over the cascaded channel power, which is a product of the channel power in the first hop and the channel power in the second hop (Chen et al. 2012). In back-scatter communications,

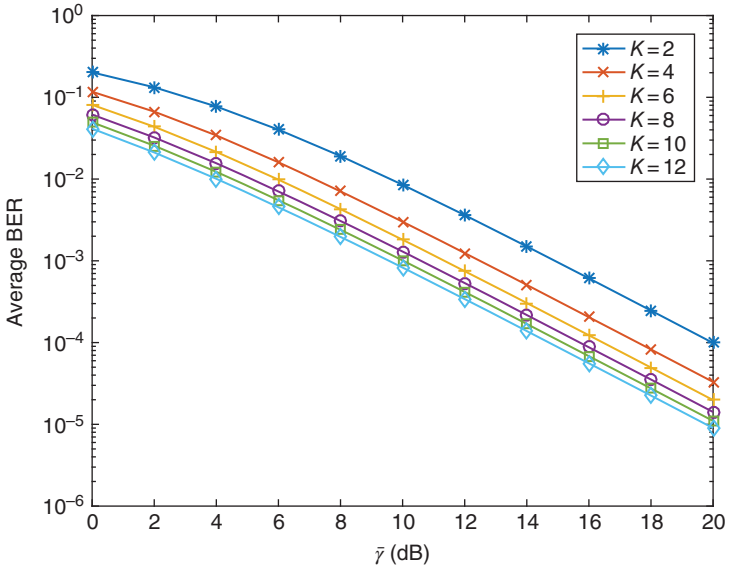

Figure 4.8 Average BER versus $\bar{\gamma}$ in Rayleigh fading channels.

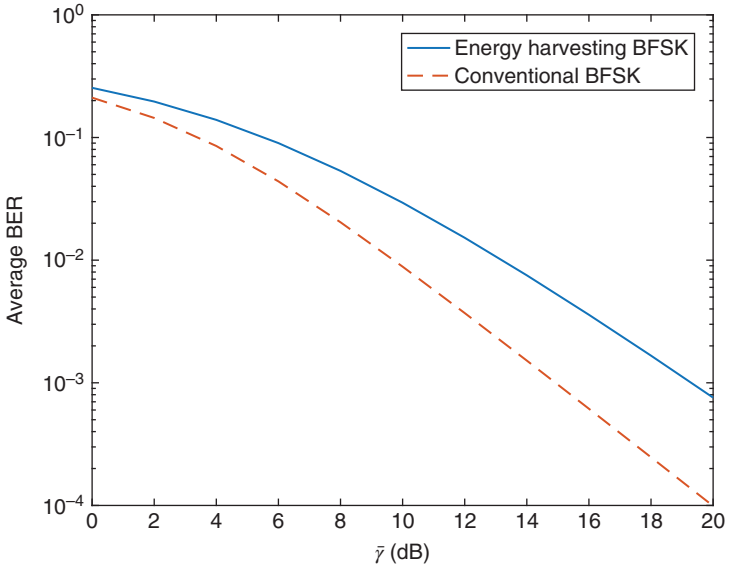

Figure 4.9 Comparison of conventional BFSK and energy harvesting BFSK in Rayleigh fading channels when $K = 1$.

the BER is averaged over the product of the forward link gain and the reverse link gain (Gao et al. 2016a). These results can be adapted to the BER analysis for energy harvesting communications.

4.2.4 Achievable Rate

For variable-power transmission, using the same SNR as in (4.17), it is easy to give the achievable rate as

$$R = \log_2(1 + \gamma P) = \log_2(1 + \epsilon). \tag{4.30}$$

Again, for conventional communications, the achievable rate only needs to be averaged over γ with P being a fixed value, while for energy harvesting communications, it needs to be averaged over both γ and P. We only need the distribution of ϵ, which has been derived in the previous subsection.

Thus, for Rayleigh fading channels, using (4.21) and (4.30), the average achievable rate is calculated as

$$\bar{R} = \int_0^\infty \log_2(1+z) f_\epsilon(z) dz = \frac{2}{(2\eta\beta^2\bar{\gamma})^{\frac{K+1}{2}}\Gamma(K)} \int_0^\infty z^{\frac{K-1}{2}} \log_2(1+z) K_{K-1}\left(2\sqrt{\frac{z}{2\eta\beta^2\bar{\gamma}}}\right) dz. \tag{4.31}$$

For Rician fading channels, using (4.26) and (4.30), similarly, the average achievable rate is

$$\bar{R} = \frac{e^{-\frac{KP_s|s|^2}{2\beta^2} - \frac{|s_d|^2}{2\alpha_d^2}}}{2\eta\beta^2\bar{\gamma}(\eta K P_s |s|^2)^{\frac{K-1}{2}}} \int_0^\infty \int_0^\infty x^{\frac{K-3}{2}} e^{-\frac{x^2}{2\eta\beta^2} - \frac{z}{x\bar{\gamma}}} I_{K-1}\left(\sqrt{\frac{KP_s|s|^2 x}{\eta\beta^4}}\right) I_0\left(\sqrt{\frac{2z|s_d|^2}{\bar{\gamma}\alpha_d^2 x}}\right) \log_2(1+z) dx dz. \tag{4.32}$$

This integration could be simplified by using the series expansion of $I_0(\cdot)$ but this will not be discussed here. Next, we use (4.31) to show the effect of energy harvesting on the achievable rate. The settings are similar to those in Figures 4.7–4.9 except that the average achievable rate is examined.

Figures 4.10 and 4.11 show the average achievable rate of energy harvesting communications. Similar to BER, the achievable rate increases with K but the increase is marginal when K is large. This can also be seen from Figure 4.11, where the rate increase from $K = 10$ to $K = 12$ is much smaller than that from $K = 2$ to $K = 4$. This suggests that the harvesting time should not be chosen too long from the capacity's point of view either. The effect of energy harvesting diminishes with the increase of K. Finally, comparing the conventional and energy harvesting communications in Figure 4.12, one sees that energy harvesting reduces the average achievable rate, which agrees with what is observed in Figure 4.9.

Note that both the BER analysis and the rate analysis show that energy harvesting can cause performance degradation but its effect diminishes with the harvesting time. This conclusion is based on the assumption that the average ϵ is the same for both conventional communications and energy harvesting communications, or the average

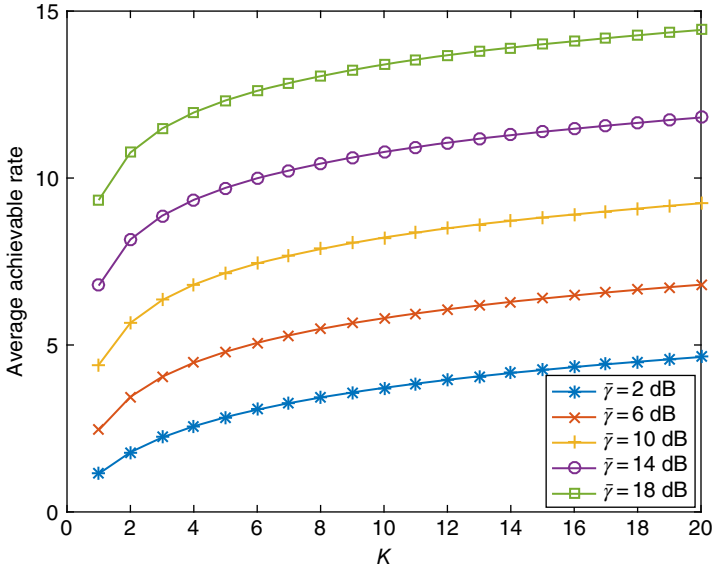

Figure 4.10 Average achievable rate (bits/s/Hz) versus K in Rayleigh fading channels.

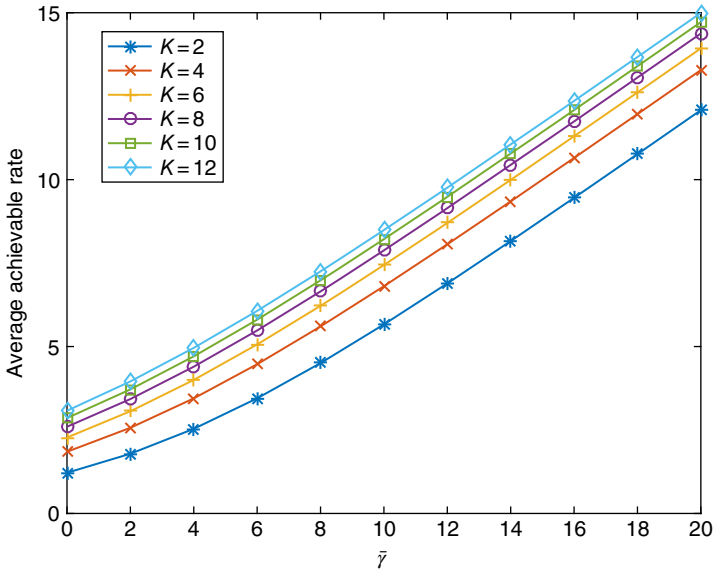

Figure 4.11 Average achievable rate (bits/s/Hz) versus $\bar{\gamma}$ in Rayleigh fading channels.

harvested power is the same as the fixed transmission power in conventional communications. In this case, the variation of power supply in energy harvesting communications is shown to degrade the system reliability or capacity. If the average harvested power is always larger than the fixed transmission power in conventional communications, these conclusions may not be valid.

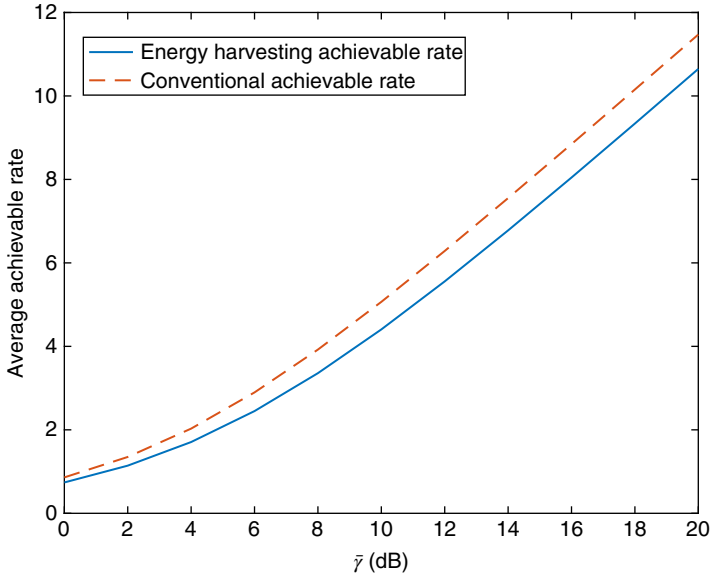

Figure 4.12 Comparison of average achievable rates (bits/s/Hz) for conventional and energy harvesting communications in Rayleigh fading channels when $K = 1$.

4.2.5 General Information Theoretic Limits

The above results have assumed energy harvesting from the RF signals. Consequently, the randomness of the power supply comes mainly from the random channel between the power source and the energy harvester. This allows us to obtain an accurate performance analysis in terms of BER and achievable rate. In a more general setting, the harvested energy can be modeled as any random process, and the randomness could come from various factors, such as the solar activity for solar power and the wind speed for wind power. In this subsection, we will give a brief discussion on how the general randomness of the power supply will affect the system capacity.

Consider a scalar AWGN channel with input X, output Y, and noise N that has zero-mean and unit-variance for simplicity. The transmission power is supplied by a battery with infinite size. The energy is harvested as a random process. In the ith channel use, an amount of E_i units will be harvested with $E\{E_i\} = \bar{E}$ as the average harvested power for all channel uses. Also, $E_i \geq 0$ and they are independent and identically distributed.

While energy is harvested, it is also used by the transmitter for data transmission. Assume that, in the ith channel use, X_i^2 units of energy are used. This gives the energy constraint as

$$\sum_{i=1}^{k} X_i^2 \leq \sum_{i=1}^{k} E_i, \ k = 1, 2, \cdots, n \tag{4.33}$$

which states that the consumed energy must be smaller than the harvested energy in any channel use. Thus, the first channel use is constrained as $X_1^2 < E_1$, the second channel use is constrained as $X_1^2 + X_2^2 < E_1 + E_2$, and so on. One sees that this energy constraint introduces memory into the channel inputs X by correlating them with each other. Thus,

in energy harvesting communications, both the dynamic power supply and the random channel introduce memory and randomness into the system, unlike conventional communications where the memory and randomness mainly come from the channel.

Define the codebook as $(n, 2^{nR_n}, \epsilon_n)$, where n is the code length, R_n is the coding rate, 2^{nR_n} is the code size, and ϵ_n is the probability of error. The messages in the set $\{1, 2, \cdots, 2^{nR_n}\}$ are equally likely. Note that an error will occur when there is a decoding error at the receiver, similar to conventional systems. However, for energy harvesting systems, an extra type of error will occur when there is an energy shortage at the transmitter due to the randomness of power supply. This can be considered as an error caused by outage. Thus, ϵ_n accounts for the probability of both errors in this case. It can be shown that the capacity of this system is upper bounded as

$$C \leq \frac{1}{2}\log_2(1 + \bar{E}) \tag{4.34}$$

where $\bar{E}$ is the average of energy arrival defined before. This upper bound can be achieved via two schemes outlined below.

In the variable-power transmission scheme discussed before, or sometimes called the "harvest-use" or "best-effort-transmit" schemes in references, the transmitter can save for $h(n)$ symbols (harvests energy only or transmits zero) first, and then it can transmit the remaining $n - h(n)$ symbols by choosing them as independent samples from a Gaussian distribution with mean zero and variance P_{avg}. It can be proved that this scheme can achieve the upper bound in (4.34) while satisfying the input constraints in (4.33) with probability arbitrarily close to one, if $P_{avg} < \bar{E}$, when $n \to \infty$. When n is finite, $\epsilon > 0$ but the capacity is still close to the upper bound. The value of $h(n)$ should be from a class of functions that scale slower than n so that both $h(n) \to \infty$ and $n - h(n) \to \infty$ when $n \to \infty$, such as $h(n) = \log(n)$. In this scheme, the transmitter does not know how much energy is harvested or available. It uses a fixed codeword.

On the other hand, in the fixed-power transmission scheme discussed before, or sometimes called the "harvest-save-use" and "save-transmit" schemes in references, the transmitter transmits if the energy at the beginning of the ith channel use is larger than the fixed transmission power X_i^2, and otherwise, it transmits a zero or keeps harvesting energy. When it transmits, it transmits a random codeword as independent samples from a Gaussian distribution with mean zero and variance P_{avg}. In this scheme, the transmitter does know how much energy is available before it decides what to transmit. This is different from the other scheme where the transmitter transmits a fixed codeword.

In both schemes, an infinite battery is assumed and circuit power consumption is ignored. More details on these schemes can be found in Ozel and Ulukus (2012). In Zenaidi et al. (2017) and other similar studies, the scheduling problem considering energy arrival has been considered. Essentially, the transmitter needs to use the harvested energy wisely based on its arrival process to avoid any energy outage. In these studies, the energy causality or the energy neutrality constraint is the key.

4.3 Energy Harvesting Detection

The physical layer lies at the bottom of a wireless system and therefore it is the most important layer in the system. The main function of the physical layer is to ensure

the reliable transmission and reception of data bits over the physical channel. Thus, an important task of the physical layer is to detect the transmitted data bits at the receiver for information decoding. Classical detectors for conventional communications systems are well studied. For example, for coherent detection of BPSK and BFSK signals, a correlator structure can be used. For non-coherent detection of BPSK signals, a differential structure can be used, and for non-coherent detection of BFSK signals, an energy detector can be used. All these detectors stem from the statistical theories based on different assumptions of channel knowledge and randomness. In energy harvesting communications, as discussed before, there is extra randomness from the power supply. Taking this extra randomness into account, new detectors are required for energy harvesting communications. In this section, we aim to derive new detectors by accounting for the characteristics of energy harvesting. Similar to the previous section, we will use RF energy harvesting as an example but the results can be easily extended to other energy sources, as long as the distributions of their transmission power are available.

Consider a simple point-to-point communications system. The received signal can be written as

$$r = g\sqrt{P_x}x + n \tag{4.35}$$

where g is the channel gain, P_x is the transmission power, x is the transmitted symbol, and n is the complex AWGN with mean zero and variance $2\sigma_d^2$. For fixed-power transmission, P_x is a fixed value. However, in order to accumulate a fixed amount of energy, the harvesting time becomes random, which leads to a random transmission delay and then a random transmission time. For variable-power transmission, $P_x = P$ is a random value. However, there is no transmission delay with fixed transmission time. Thus, either the transmission power or the transmission time are random in energy harvesting communications. In the following, we only consider the variable-power transmission where $P_x = P$. This gives

$$r = g\sqrt{P}x + n. \tag{4.36}$$

If both g and P are known via channel estimation at the receiver, for BPSK with $x = \pm 1$, the likelihood function can be derived as

$$f(r|x = \pm 1) = \frac{1}{2\pi\sigma_d^2} e^{-\frac{|r \mp \sqrt{P}g|^2}{2\sigma_d^2}}. \tag{4.37}$$

Using the likelihood ratio test and assuming equal probabilities for $x = +1$ and $x = -1$, one has

$$\frac{f(r|x=+1)}{f(r|x=-1)} \underset{-1}{\overset{+1}{\gtrless}} 1 \tag{4.38}$$

and the coherent detector for BPSK is derived as

$$\Re\{r \cdot g^*\} \underset{-1}{\overset{+1}{\gtrless}} 0 \tag{4.39}$$

where $\Re\{\cdot\}$ takes the real part of a complex number. This detector is the same as the coherent detector for BPSK in conventional communications (Proakis 2001). If BFSK

is used, one has $x = 0$ or $x = \sqrt{2}$ with equal probabilities. The reason for using $x = \sqrt{2}$ instead of $x = 1$ is to ensure the same average power for both BFSK and BPSK in the comparison. In this case, the likelihood functions can be derived as

$$f(r|x=0) = \frac{1}{2\pi\sigma_d^2} e^{-\frac{|r|^2}{2\sigma_d^2}} \tag{4.40}$$

$$f(r|x=\sqrt{2}) = \frac{1}{2\pi\sigma_d^2} e^{-\frac{|r-\sqrt{2P}g|^2}{2\sigma_d^2}}. \tag{4.41}$$

Using them in the likelihood ratio test, one has

$$\Re\{r \cdot g^*\} \underset{0}{\overset{\sqrt{2}}{\gtrless}} \sqrt{\frac{P}{2}}|g|^2. \tag{4.42}$$

The above detector is again the same as that in conventional communications without energy harvesting.

Next, we discuss several special cases when the detectors for energy harvesting are different. In the first special case, if g is known via channel estimation at the receiver but the transmission power P is unknown, the likelihood function in this case can be derived as

$$\begin{aligned} f(r|x=\pm 1) &= \frac{1}{2\pi\sigma_d^2} \int_0^\infty e^{-\frac{|r\mp\sqrt{y}g|^2}{2\sigma_d^2}} f_P(y)dy. \\ &= \frac{e^{-\frac{|r|^2}{2\sigma_d^2}}}{2\pi\sigma_d^2} \int_0^\infty e^{-\frac{|g|^2}{2\sigma_d^2}y \pm \frac{\Re\{rg^*\}}{\sigma_d^2}\sqrt{y}} f_P(y)dy. \end{aligned} \tag{4.43}$$

When the channel from the power source to the energy harvester suffers from Rayleigh fading, the PDF of P is given by (4.10). Using (4.10) in (4.43), solving the integral using an equation in Gradshteyn and Ryzhik (2000, eq. (3.462.1)), and finally applying the solved integral in the likelihood ratio test (4.38), one has the new coherent detector for BPSK with unknown transmission power as

$$\frac{D_{-2K}\left(-\dfrac{\Re\{r \cdot g^*\}}{\sigma_d\sqrt{|g|^2 + \sigma_d^2/(\eta\beta^2)}}\right)}{D_{-2K}\left(\dfrac{\Re\{r \cdot g^*\}}{\sigma_d\sqrt{|g|^2 + \sigma_d^2/(\eta\beta^2)}}\right)} \underset{-1}{\overset{+1}{\gtrless}} 1 \tag{4.44}$$

where $D(\cdot)$ is the parabolic cylinder function Gradshteyn and Ryzhik (2000, eq. (9.240)) by solving the integration in (4.43) and all the other symbols are defined as before. Further, if one uses the expression of the parabolic cylinder function in Gradshteyn and Ryzhik (2000, eq. (9.240)), it can be shown that (4.44) is equivalent to (4.39). This is expected, as for phase modulation, the amplitude does not affect the performance and

hence it does not matter whether P is known or unknown. One can use a similar method to derive the new detector for Rician fading channels. The derivation is omitted here. For BFSK, the likelihood function for $x = \sqrt{2}$ in a Rayleigh fading channel is derived as

$$\begin{aligned} f(r|x=\sqrt{2}) &= \frac{1}{2\pi\sigma_d^2}\int_0^\infty e^{-\frac{|r-\sqrt{2}yg|^2}{2\sigma_d^2}} f_P(y)dy \\ &= \frac{e^{-\frac{|r|^2}{2\sigma_d^2}}}{2\pi\sigma_d^2}\int_0^\infty e^{-\frac{|g|^2}{\sigma_d^2}y+\frac{\sqrt{2}y\Re\{rg^*\}}{\sigma_d^2}} f_P(y)dy \\ &= \frac{2e^{-\frac{|r|^2}{2\sigma_d^2}}\Gamma(2K)e^{\frac{\Re^2\{rg^*\}}{4|g|^2\sigma_d^2+2\sigma_d^4/(\eta\beta^2)}}}{2\pi\sigma_d^2(2\eta\beta^2)^K\Gamma(K)\left(\frac{2|g|^2}{\sigma_d^2}+\frac{1}{\eta\beta^2}\right)^K} D_{-2K}\left(-\frac{\Re\{rg^*\}}{\sqrt{|g|^2\sigma_d^2+\sigma_d^4/(2\eta\beta^2)}}\right) \end{aligned} \tag{4.45}$$

where we have used the equation in Gradshteyn and Ryzhik (2000, eq. (3.462.1)) again. Then, the new coherent detector for BFSK in energy harvesting communications with unknown transmission power can be derived as

$$\frac{2\Gamma(2K)e^{\frac{\Re^2\{rg^*\}}{4|g|^2\sigma_d^2+2\sigma_d^4/(\eta\beta^2)}}}{(2\eta\beta^2)^K\Gamma(K)\left(\frac{2|g|^2}{\sigma_d^2}+\frac{1}{\eta\beta^2}\right)^K} D_{-2K}\left(-\frac{\Re\{rg^*\}}{\sqrt{|g|^2\sigma_d^2+\sigma_d^4/(2\eta\beta^2)}}\right) \underset{0}{\overset{\sqrt{2}}{\gtrless}} 1. \tag{4.46}$$

In another special case, if g is unknown but P is known, using the likelihood ratio test and assuming that the channel gain is complex Gaussian with mean zero and variance $2\alpha_d^2$, one has the non-coherent detector for BFSK as

$$|r|^2 \underset{0}{\overset{\sqrt{2}}{\gtrless}} \frac{(\sigma_d^2+2P\alpha_d^2)\sigma_d^2}{P\alpha_d^2}\ln\left[\frac{\sigma_d^2+2P\alpha_d^2}{\sigma_d^2}\right] \tag{4.47}$$

which is the traditional energy detector.

When both g and P are unknown, for energy harvesting communications, the new non-coherent detector for BFSK can be derived as

$$\frac{\sigma_d^2 e^{\frac{|r|^2}{2\sigma_d^2}}}{(2\eta\beta^2)^K\Gamma(K)}\int_0^\infty \frac{x^{K-1}}{\sigma_d^2+2\alpha_d^2 x}e^{-\frac{x}{2\eta\beta^2}-\frac{|r|^2}{2(\sigma_d^2+2\alpha_d^2 x)}}dx \underset{0}{\overset{\sqrt{2}}{\gtrless}} 1. \tag{4.48}$$

The integration does not have a closed-form expression but simplification is possible when the average SNR $\frac{\alpha_d^2}{\sigma_d^2}$ is very large. For BPSK, the non-coherent detector requires differential encoding at the transmitter. The derivation is similar to the above, albeit more complicated. It is not presented here.

The above results are only applicable to binary signaling. However, one can easily extend them to M-ary signaling by calculating the likelihood function for each transmitted symbol. Also, we have only considered RF energy harvesting, where the

distribution of the harvested power or the power supply is derived in Section 4.2.1 as either a central chi-square distribution or a non-central chi-square distribution. For other harvesting techniques, as long as the distribution of the harvested power is available, similar detectors can be obtained. Next, we show the performances of the newly derived detectors for RF energy harvesting communications using BFSK and $\eta = 0.5$. Figure 4.13 compares the coherent detector for conventional communications in (4.42) with that for energy harvesting communications in (4.46), where K is the number of time slots used for harvesting. Figure 4.14 compares the non-coherent detector for conventional communications in (4.47) with that for energy harvesting communications in (4.48).

One sees from these two figures that the detector in conventional communications always outperforms that in energy harvesting communications, due to the extra variation in power supply for energy harvesting communications. This agrees with our observations before. However, the performance difference is very small for the non-coherent detectors. Also, the difference decreases when K increases. Statistically, when the shape parameter K increases, the Gamma distribution of the harvested power in Rayleigh fading channels becomes more impulsive so that less variation will occur.

The above discussion has presented some very simple results on how new detectors can be designed for energy harvesting communications. Recall that for conventional communications the randomness mainly comes from the communications channel, while for energy harvesting communications the randomness comes from both the communications channel and the power supply. Thus, in most cases, the extra randomness from the power supply needs to be considered for efficient detection of signals in energy harvesting communications.

Bearing this main difference in mind, one can easily obtain results for energy harvesting communications in other cases. For example, if imperfect channel knowledge

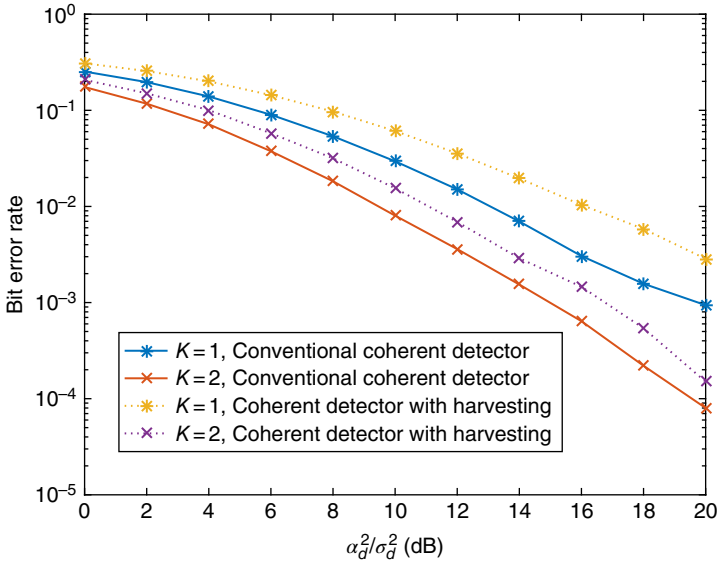

Figure 4.13 Comparison of conventional and energy harvesting communications using coherent detectors.

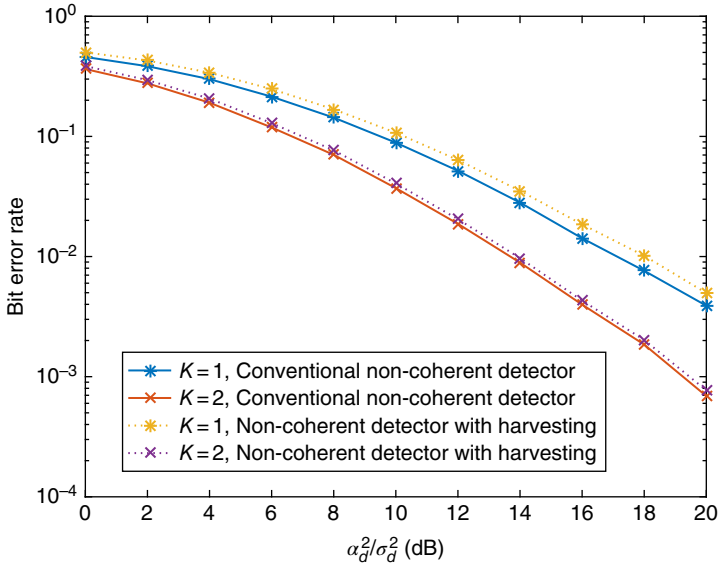

Figure 4.14 Comparison of conventional and energy harvesting communications using non-coherent detectors.

is considered due to channel estimation errors, one may introduce extra errors in the estimation of the transmission power too for a similar discussion. Also, there will be four cases, known channel and known transmission power, known channel and unknown transmission power, unknown channel and known transmission power, and unknown channel and unknown transmission power, for energy harvesting communications. Finally, detectors for the fixed-power transmission schemes can be derived too. These schemes have a fixed transmission power but a random transmission time. Both fixed-power transmission and variable-power transmission depend on the random energy arrival process.

Note that, in the general case, the random channel should be independent of the random power source. For example, if solar-powered devices are used for radio communications, the randomness of the power supply comes from the solar activities, while the randomness of the channel comes from fading and noise. However, in some cases, the random channel and the random power source may be correlated. For example, if both power transfer and information transmission share the same radio channel, the fading h_k in y_k in (4.1) may be correlated with the fading g in r in (4.35) so that P might be correlated with g in the detection. This is the case in wireless powered communications. Assume that the fading channel remains the same during power transfer and information transmission such that $h_k = g$ for $k = 1, 2, \cdots, K$. In this case,

$$y_k = g\sqrt{P_s}s_k + n_k. \tag{4.49}$$

Thus, conditioned on g, the PDF of the harvested power P will become a non-central chi-square distribution with PDF

$$f_P(y) = \frac{e^{-\frac{y}{2\eta\sigma^2} - \frac{KP_s|g|^2|s|^2}{2\sigma^2}}}{2\eta\sigma^2(\eta K P_s|g|^2|s|^2)^{\frac{K-1}{2}}} y^{\frac{K-1}{2}} I_{K-1}\left(\sqrt{\frac{KP_s|g|^2|s|^2 y}{\eta\sigma^4}}\right) \tag{4.50}$$

for any fading channels. This PDF can then be used to calculate the likelihood function when P is unknown but g is known in (4.44) and (4.46), etc. These likelihood functions will lead to different detectors. Details of these derivations are omitted here. The method is the same as before. Some similar studies have also been conducted in Liu et al. (2015a) for wireless relaying systems with two hops.

In summary, two important issues in energy harvesting detection are the extra randomness from the power supply and the relationship between this extra randomness and the usual channel randomness. They lead to new and different detector designs. Indeed, these two issues also affect the performances of other physical layer techniques, such as channel estimation, which will be discussed in the next section.

4.4 Energy Harvesting Estimation

In this section, we discuss another important physical layer technique, channel estimation. Most modern communications systems acquire channel knowledge via channel estimation in order to provide satisfactory QoS for users. There are many different types of channel estimators, depending on the channel conditions and system requirements. The most reliable channel estimators are pilot-based estimators, where the transmitter sends a number of known pilot symbols embedded as part of the header in the data frame and the receiver uses the received signals of the known pilot symbols for channel estimation to detect the received data symbols in the same or different frames (Chen and Beaulieu 2007). Several important issues arise in energy harvesting estimation.

First, channel estimator designs often depend on the statistics of the received pilot symbols. If the transmitter has used the dynamic harvested power in energy harvesting communications to transmit the pilot symbols, in the received pilot symbols, in addition to the channel randomness, one also has the extra randomness from the power supply. Consequently, the statistics of the received pilot symbols will change so that channel estimators for conventional communications cannot be used. Take r in (4.46) as an example. Assume that the received pilot symbols are given by

$$r_i = g\sqrt{P}x_i + n_i \tag{4.51}$$

where $x_i = 1$ is the pilot value and $i = 1, 2, \cdots, I$ index the pilot symbols. In the conventional communications, the only randomness comes from n_i. The moment-based (MB) estimator for g can be easily derived as

$$\hat{g} = \frac{1}{I\sqrt{P}} \sum_{i=1}^{I} r_i. \tag{4.52}$$

In energy harvesting communications, $\sqrt{P}$ is random too so that (4.52) cannot be used directly. Instead, $\sqrt{P}$ should be replaced by its average $E\{\sqrt{P}\}$ in (4.52) to give

$$\hat{g} = \frac{1}{IE\{\sqrt{P}\}} \sum_{i=1}^{I} r_i \tag{4.53}$$

where $E\{\cdot\}$ denotes the expectation operation. Similarly, for maximum likelihood (ML) estimators, minimum mean squared error (MSE) estimators and other estimation

methods, the extra randomness from P needs to be considered for energy harvesting communications. This process is very similar to that in the previous section for signal detection. This will not be discussed further here.

Secondly, if the random power source and the random channel are independent but channel estimation and energy harvesting are performed by the same remote device, the addition of the energy harvesting capability may reduce the system resources for other tasks. For example, in the conventional communications, for a data frame with fixed length, one has to allocate the number of symbols between channel estimation and data transmission. In energy harvesting communications, if the data frame still has a fixed length, one has to allocate the number of symbols between channel estimation, energy harvesting and data transmission now, similar to the work in Wang et al. (2014). Also, if the random power source and the random channel are correlated, such as in wireless powered communications, energy harvesting and channel estimation might be correlated. In this case, the signals for energy harvesting contain the same channel gain to be estimated and thus this information can be shared to improve estimation accuracy.

Next, we will focus on the second issue. This will be first studied in the context of a wireless relaying system, where each communication is performed in two hops: from source to relay; and from relay to destination. In energy harvesting channel estimation, the transmission of the pilot symbols in the second hop is powered by energy harvested from the first hop. Then, a one-hop system without relaying will be discussed.

4.4.1 With Relaying

Consider a wireless relaying network with one source, one relay and one destination. The signal is transmitted from the source to the destination via the relay. There is no direct link between the source and the destination. Assume that a total of K pilots are used for both energy harvesting and channel estimation. Each pilot occupies a time duration of T_p. We consider six schemes of energy harvesting channel estimation.

4.4.1.1 Scheme 1

In Scheme 1, the relay node obtains energy from the source that requires the channel state information. The harvested energy will be used by the relay node to forward pilots from the source node and transmit extra pilots to the destination node so that channel estimation can be performed. In this case, energy harvesting estimation works in the following way.

First, one has the source node that will transmit I pilots to the relay node for energy harvesting. The received signals of these pilots are given by

$$y_{r-eh}^{(i)} = \sqrt{P_s} hs + n_{r-eh}^{(i)} \tag{4.54}$$

where $i = 1, 2, \cdots, I$, P_s is the transmission power of the source node, h is the channel coefficient of the source-to-relay link and is a complex Gaussian random variable with mean zero and variance $2\alpha^2$, s is the pilot value and it is assumed that $s = 1$ in the following, and n_{r-eh} is the AWGN with mean zero and variance $2\sigma^2$. All the noise in this section is assumed circularly symmetric. Using (4.54), the harvested energy is

$$E_h = \eta P_s |h|^2 I T_p \tag{4.55}$$

where η is the conversion efficiency of the energy harvester that has been discussed in Chapter 3 and IT_p is the total time for energy harvesting. Note that $P_s|h|^2$ is the amount

of radiated power from the source node picked up by the harvester as its input. Due to path loss and fading, this amount is often small.

In the second step, the source node will transmit another J_1 pilots to the relay node. These pilots will be forwarded to the destination for channel estimation using the harvested energy. The received signals of these pilots at the destination is

$$y_{d-s}^{(j_1)} = \sqrt{P_r} g a y_{r-ce}^{(j_1)} + n_{d-s}^{(j_1)}, \tag{4.56}$$

where $y_{r-ce}^{(j_1)} = \sqrt{P_s} h + n_{r-ce}^{(j_1)}$ is the pilot that is forwarded by the relay, $j_1 = 1, 2, \cdots, J_1$, $n_{r-ce}^{(j_1)}$ is the AWGN at the relay, P_r is the transmission power of the relay node that will be calculated later, g is the channel coefficient of the relay-to-destination link and it is a complex Gaussian random variable with mean zero and variance $2\alpha^2$, a is the amplification factor, and $n_{d-s}^{(j_1)}$ is the AWGN at the destination. Both $n_{r-ce}^{(j_1)}$ and $n_{d-s}^{(j_1)}$ are complex Gaussian with mean zero and variance $2\sigma^2$. This chapter assumes identical noise variances for the relay and the destination. This is the case when the source, the relay and the destination are peer nodes in the network such that they have similar receivers. Nevertheless, it is also straightforward to extend the result to the case when the relay and the destination have different noise variances. In Scheme 1, since the relay node does not perform channel estimation, fixed-gain relaying can be used such that one can set a as a constant for simplicity.

Finally, the relay node also uses the harvested energy to transmit J_2 pilots from its own to the destination, and their received signals are given by

$$y_{d-r}^{(j_2)} = \sqrt{P_r} g + n_{d-r}^{(j_2)} \tag{4.57}$$

where $j_2 = 1, 2, \cdots, J_2$, $n_{d-r}^{(j_2)}$ is the AWGN at the destination and is again complex Gaussian with mean zero and variance $2\sigma^2$. This signal only has the pilot value and it does not have any forwarded signal. The relay uses the harvested energy in (4.55) to forward J_1 pilots from the source node and transmit J_2 pilots of its own. Thus, the transmission power of the relay can be written as

$$P_r = \frac{E_h}{JT_p} = \eta P_s |h|^2 \frac{I}{J} \tag{4.58}$$

where $J = J_1 + J_2$. Using $y_{d-s}^{(j_1)}$ in (4.56) and $y_{d-r}^{(j_2)}$ in (4.57), we can estimate the channel coefficients g and h.

From (4.57), one has

$$y_{d-r}^{(j_2)} = \sqrt{\eta \frac{I}{J} P_s} |h| g + n_{d-r}^{(j_2)} \tag{4.59}$$

and from (4.56), one has

$$y_{d-s}^{(j_1)} = \sqrt{\eta \frac{I}{J} P_s} |h| g h a + \sqrt{\eta \frac{I}{J} P_s} |h| g a n_{r-ce}^{(j_1)} + n_{d-s}^{(j_1)}. \tag{4.60}$$

It is well-known that the MB estimators are often simpler than other estimators. In some cases, they also provide efficient estimation. Thus, they are considered first. The first-order moments of (4.59) and (4.60) are

$$E\{y_{d-r}^{(j_2)}\} = \sqrt{\eta \frac{I}{J} P_s} |h| g \tag{4.61}$$

$$E\{y_{d-s}^{(j_1)}\} = \sqrt{\eta \frac{I}{J} P_s}|h|gha. \tag{4.62}$$

One can approximate $E\{y_{d-r}^{(j_2)}\}$ using $\frac{1}{J_2}\sum_{j_2=1}^{J_2} y_{d-r}^{(j_2)}$. Also, the value of $E\{y_{d-s}^{(j_1)}\}$ can be approximated as $\frac{1}{J_1}\sum_{j_1=1}^{J_1} y_{d-s}^{(j_1)}$. Solving the equations in (4.61) and (4.62) for g and h, one has the MB estimators for g and h in Scheme 1 as

$$\hat{g}_1 = \frac{\frac{1}{J_2}\sum_{j_2=1}^{J_2} y_{d-r}^{(j_2)} | \frac{1}{J_2}\sum_{j_2=1}^{J_2} y_{d-r}^{(j_2)}|}{\frac{1}{a}\sqrt{\eta \frac{I}{J}} | \frac{1}{J_1}\sum_{j_1=1}^{J_1} y_{d-s}^{(j_1)}|} \tag{4.63}$$

$$\hat{h}_1 = \frac{1}{\sqrt{P_s}a} \frac{\frac{1}{J_1}\sum_{j_1=1}^{J_1} y_{d-s}^{(j_1)}}{\frac{1}{J_2}\sum_{j_2=1}^{J_2} y_{d-r}^{(j_2)}}, \tag{4.64}$$

respectively. Note that other orders of moments can also be used but the lower the order of moment is, the better the MB estimator will be. Thus, we use the first order.

The ML estimators can be derived as in the following. Denote $G_y = \sqrt{\eta \frac{I}{J} P_s}|h|g$. Using (4.57) and the ML method, the log-likelihood function can be derived as

$$llf_1 = -J_2 \ln(2\pi\sigma_d^2) - \frac{1}{2\sigma_d^2}\sum_{j_2=1}^{J_2} |y_{d-r}^{(j_2)} - G_y|^2. \tag{4.65}$$

Thus, by differentiating (4.65) with respect to G_y, setting the derivative to zero and solving the equation for G_y, the ML estimate of G_y can be derived as

$$\hat{G}_y = \frac{1}{J_2}\sum_{j_2=1}^{J_2} y_{d-r}^{(j_2)} = \sqrt{\eta \frac{I}{J} P_s}|\hat{h}|\hat{g}. \tag{4.66}$$

Also, denote $H_y = \sqrt{P_s}h$. Using (4.60) and the ML method, another log-likelihood function can be derived as

$$\begin{aligned} llf_2 = &-J_1 \ln(2\pi(1 + |G_y|^2 a^2)\sigma_d^2) \\ &- \frac{1}{2(1 + |G_y|^2 a^2)\sigma_d^2}\sum_{j_1=1}^{J_1} |y_{d-s}^{(j_1)} - G_y H_y a|^2. \end{aligned} \tag{4.67}$$

By differentiating (4.67) with respect to H_y, setting the derivative to zero and solving the equation for H_y, the ML estimate of H_y can be derived as

$$\hat{H}_y = \frac{1}{J_1 \hat{G}_y a}\sum_{j_1=1}^{J_1} y_{d-s}^{(j_1)} = \sqrt{P_s}\hat{h}. \tag{4.68}$$

The invariance principle of ML estimation states that a function of ML estimate is the ML estimate of that function. Using this principle, the ML estimates of g and h can be derived by solving (4.66) and (4.68) for $\hat{g}$ and $\hat{h}$, which are the same as the MB estimators using the first-order moments. Thus, results for the MB estimators are also applicable to the ML estimators. Since both $y_{d-s}^{(j_1)}$ and $y_{d-r}^{(j_2)}$ are samples received at the destination,

in this scheme, the relay does not perform channel estimation. Only the destination performs channel estimation. This reduces the complexity at the relay, which is desirable to encourage idle nodes to take part in relaying. The first- and second-order moments of the estimates can also be derived.

For Scheme 1, denote $y_r = \frac{1}{J_2}\sum_{j_2=1}^{J_2} y_{d-r}^{(j_2)} = r_{y_r} e^{j\theta_{y_r}}$ and $y_s = \frac{1}{J_1}\sum_{j_1=1}^{J_1} y_{d-s}^{(j_1)} = r_{y_s} e^{j\theta_{y_s}}$. One sees that y_r and y_s are complex Gaussian random variables with means $S_{y_r} = \sqrt{\eta_J^I P_s}|h|g$ and $S_{y_s} = \sqrt{\eta_J^I P_s}|h|ghha$ and variances $2\beta_{y_r}^2 = \frac{2\sigma^2}{J_2}$ and $2\beta_{y_s}^2 = \frac{2\sigma^2}{J_1}(1+\eta_J^I P_s|h|^2|g|^2a^2)$, respectively. Hence, r_{y_r} and r_{y_s} are Rician random variables.

From (4.63), one has

$$E\{\hat{g}_1\} = \frac{a}{\sqrt{\eta_J^I}} E\{r_{y_r}^2 e^{j\theta_{y_r}}\} E\left\{\frac{1}{r_{y_s}}\right\} \tag{4.69}$$

where

$$E\{r_{y_r}^2 e^{j\theta_{y_r}}\} = \frac{3\beta_{y_r}^2}{e^{\frac{|S_{y_r}|^2}{2\beta_{y_r}^2}}\sqrt{\pi}} \int_0^{2\pi} e^{j\theta_{y_r} + \frac{|S_{y_r}|^2\cos^2(\theta_{y_r}+\epsilon)}{4\beta_{y_r}^2}} D_{-4}\left(-\frac{|S_{y_r}|\cos(\theta_{y_r}+\epsilon)}{\beta_{y_r}}\right) d\theta_{y_r} \tag{4.70}$$

using Gradshteyn and Ryzhik (2000, eq. (3.462.1)) and Stuber (2001, eq. (A.29))

$$E\left\{\frac{1}{r_{y_s}}\right\} = \frac{\sqrt{\pi} e^{-\frac{|S_{y_s}|^2}{4\beta_{y_s}^2}}}{\sqrt{2\beta_{y_s}^2}} I_0\left(\frac{|S_{y_s}|^2}{4\beta_{y_s}^2}\right) \tag{4.71}$$

using Gradshteyn and Ryzhik (2000, eq. (6.618.4)) and Stuber (2001, eq. (2.45)), ϵ is the negative of the phase angle of g, $D_{-4}(\cdot)$ is the parabolic cylinder function (Gradshteyn and Ryzhik 2000, eq. (9.240)) and $I_0(\cdot)$ is the zeroth-order modified Bessel function of the first kind (Gradshteyn and Ryzhik 2000 eq. (8.406.1)).

Also, from (4.64), one has

$$E\{\hat{h}_1\} = \frac{S_{y_s}}{\sqrt{P_s}a} E\left\{\frac{1}{r_{y_r}} e^{-j\theta_{y_r}}\right\} \tag{4.72}$$

where

$$E\left\{\frac{e^{-j\theta_{y_r}}}{r_{y_r}}\right\} = \frac{1}{\sqrt{2\pi\beta_{y_r}^2}} \int_0^{2\pi} e^{-j\theta_{y_r} - \frac{|S_{y_r}|^2\sin^2(\theta_{y_r}+\epsilon)}{2\beta_{y_r}^2}} Q(-|S_{y_r}|\cos(\theta_{y_r}+\epsilon)/\beta_{y_r}) d\theta_{y_r} \tag{4.73}$$

and $Q(\cdot)$ is the Gaussian Q function. The second-order moments can be derived in the following.

From (4.63), one has

$$E\{|\hat{g}_1|^2\} = \frac{a^2}{\eta_J^I} E\{r_{y_r}^4\} E\left\{\frac{1}{r_{y_s}^2}\right\} \tag{4.74}$$

where

$$E\{r_{y_r}^4\} = 2(2\beta_{y_r}^2)^2 + 4(2\beta_{y_r}^2)|S_{y_r}|^2 + |S_{y_r}|^4 \tag{4.75}$$

using moments of a Rician random variable and

$$E\left\{\frac{1}{r_{y_s}^2}\right\} = \int_0^\infty \frac{1}{\beta_{y_s}^2 x} e^{-\frac{x^2+|S_{y_s}|^2}{2\beta_{y_s}^2}} I_0\left(\frac{x|S_{y_s}|}{\beta_{y_s}^2}\right) dx \tag{4.76}$$

using Stuber (2001, eq. (2.45)). Also, from (4.64), one has

$$E\{|\hat{h}_1|^2\} = \frac{1}{P_s a^2} E\{r_{y_s}^2\} E\left\{\frac{1}{r_{y_r}^2}\right\} \tag{4.77}$$

where

$$E\{r_{y_s}^2\} = 2\beta_{y_s}^2 + |S_{y_s}|^2 \tag{4.78}$$

and

$$E\left\{\frac{1}{r_{y_r}^2}\right\} = \int_0^\infty \frac{1}{\beta_{y_r}^2 x} e^{-\frac{x^2+|S_{y_r}|^2}{2\beta_{y_r}^2}} I_0\left(\frac{x|S_{y_r}|}{\beta_{y_r}^2}\right) dx. \tag{4.79}$$

4.4.1.2 Scheme 2

Scheme 2 works in a similar way to Scheme 1, but Scheme 2 harvests the energy by splitting the signal in the power domain. Details of these energy harvesting strategies can also be found in Chapter 6. First, the source transmits K_1 pilots to the relay. The received signal at the relay is divided into two parts. One part is used for channel estimation as $z_{r-ce}^{(k_1)} = \sqrt{(1-\rho)P_s}h + n_{r-ce}^{(k_1)}$, which is forwarded to the destination to give

$$z_{d-s}^{(k_1)} = \sqrt{P_r} g a z_{r-ce}^{(k_1)} + n_{d-s}^{(k_1)} \tag{4.80}$$

where $k_1 = 1, 2, \cdots, K_1$ index the pilots from the source, ρ is the important power splitting factor, $n_{r-ce}^{(k_1)}$ and $n_{d-s}^{(k_1)}$ are the AWGN with means zero and variances $2\sigma_r^2$ and $2\sigma_d^2$, respectively. Another part of the received signal at the relay is harvested as $E_h = \eta\rho P_s |h|^2 K_1 T_p$.

Secondly, the relay also transmits K_2 own pilots to the destination such that the received signal at the destination is

$$z_{d-r}^{(k_2)} = \sqrt{P_r} g + n_{d-r}^{(k_2)} \tag{4.81}$$

where $k_2 = 1, 2, \cdots, K_2$ and $n_{d-r}^{(k_2)}$ is the AWGN with mean zero and variance $2\sigma_d^2$.

Since the relay forwards K_1 pilots from the source and also transmits K_2 pilots from itself, a total of $K = K_1 + K_2$ pilots will be received at the destination as

$$P_r = \frac{E_h}{K T_p} = \eta\rho P_s |h|^2 \frac{K_1}{K}. \tag{4.82}$$

Thus, one can obtain

$$z_{d-r}^{(k_2)} = \sqrt{\eta\rho P_s \frac{K_1}{K}} |h| g + n_{d-r}^{(k_2)} \tag{4.83}$$

and

$$z_{d-s}^{(k_1)} = \sqrt{\eta\rho(1-\rho)\frac{K_1}{K}} P_s |h| g h a + \sqrt{\eta\rho P_s \frac{K_1}{K}} |h| g a n_{r-ce}^{(k_1)} + n_{d-s}^{(k_1)}. \tag{4.84}$$

The MB estimators are derived first. One has the first-order moments of $z_{d-r}^{(k_2)}$ and $z_{d-s}^{(k_1)}$ as

$$E\{z_{d-r}^{(k_2)}\} = \sqrt{\eta\rho P_s \frac{K_1}{K}}|h|g \tag{4.85}$$

$$E\{z_{d-s}^{(k_1)}\} = \sqrt{\eta\rho(1-\rho)\frac{K_1}{K}P_s}|h|gha. \tag{4.86}$$

Thus, it is quite straightforward to derive the MB estimators for g and h from (4.85) and (4.86) as

$$\hat{g}_2 = \frac{a\sqrt{1-\rho}}{\sqrt{\eta\rho\frac{K_1}{K}}} \frac{\frac{1}{K_2}\sum_{k_2=1}^{K_2} z_{d-r}^{(k_2)}|\frac{1}{K_2}\sum_{k_2=1}^{K_2} z_{d-r}^{(k_2)}|}{|\frac{1}{K_1}\sum_{k_1=1}^{K_1} z_{d-s}^{(k_1)}|} \tag{4.87}$$

and

$$\hat{h}_2 = \frac{1}{\sqrt{(1-\rho)P_s}a} \frac{\frac{1}{K_1}\sum_{k_1=1}^{K_1} z_{d-s}^{(k_1)}}{\frac{1}{K_2}\sum_{k_2=1}^{K_2} z_{d-r}^{(k_2)}}, \tag{4.88}$$

respectively.

The ML estimators are derived in the following. Denote $G_z = \sqrt{\eta\rho P_s \frac{K_1}{K}}|h|g$ and $H_z = \sqrt{(1-\rho)P_s}h$. Similar to before, using the ML method, the ML estimate of G_z can be derived as

$$\hat{G}_z = \frac{1}{K_2}\sum_{k_2=1}^{K_2} z_{d-r}^{(k_2)} = \sqrt{\eta\rho P_s \frac{K_1}{K}}|\hat{h}|\hat{g} \tag{4.89}$$

and using the ML method, the ML estimate of H_z can be derived as

$$\hat{H}_z = \frac{1}{K_1\hat{G}_z a}\sum_{k_1=1}^{K_1} z_{d-s}^{(k_1)} = \sqrt{(1-\rho)P_s}\hat{h}. \tag{4.90}$$

Using the invariance principle, the ML estimators for g and h can be obtained by solving (4.89) and (4.90), which are the same as the MB estimators using the first-order moments. Again, only the destination needs to perform channel estimation to reduce complexity at the relay. The ML estimation and the MB estimator are the same for both Scheme 1 and Scheme 2. From here on, we will not derive them separately and will only focus on the simpler MB estimators.

Next, we derive the first- and second-order moments of $\hat{g}_2$ and $\hat{h}_2$. Denote $z_r = \frac{1}{K_2}\sum_{k_2=1}^{K_2} z_{d-r}^{(k_2)} = r_{z_r}e^{j\theta_{z_r}}$ and $z_s = \frac{1}{K_1}\sum_{k_1=1}^{K_1} z_{d-s}^{(k_1)} = r_{z_s}e^{j\theta_{z_s}}$, which are complex Gaussian random variables with means $S_{z_r} = \sqrt{\eta\rho P_s \frac{K_1}{K}}|h|g$ and $S_{z_s} = \sqrt{\eta\rho(1-\rho)\frac{K_1}{K}P_s}|h|gha$ and variances $2\beta_{z_r}^2 = \frac{2\sigma^2}{K_2}$ and $2\beta_{z_s}^2 = \frac{2\sigma^2}{K_1}(1+\eta\rho P_s|h|^2|g|^2a^2\frac{K_1}{K})$, respectively.

From (4.87), the first-order moment of $\hat{g}_2$ can be derived as

$$E\{\hat{g}_2\} = \frac{a}{\sqrt{\eta\frac{K_1}{K}}}\sqrt{\frac{1-\rho}{\rho}}E\{r_{z_r}^2 e^{j\theta_{z_r}}\}E\{\frac{1}{r_{z_s}}\} \tag{4.91}$$

where $E\{r_{z_r}^2 e^{j\theta_{z_r}}\}$ and $E\{\frac{1}{r_{z_s}}\}$ are similar to those in Scheme 1, except that S_{y_r}, β_{y_r}, S_{y_s}, and β_{y_s} are replaced by S_{z_r}, β_{z_r}, S_{z_s}, and β_{z_s}, respectively. The first-order moment of $\hat{h}_2$ is derived from (4.88) as

$$E\{\hat{h}_2\} = \sqrt{\eta\rho P_s \frac{K_1}{K}}|h|ghE\left\{\frac{1}{r_{z_r}} e^{-j\theta_{z_r}}\right\} \tag{4.92}$$

where $E\{\frac{1}{r_{z_r}} e^{-j\theta_{z_r}}\}$ is similar to before except that S_{y_r} and β_{y_r} are replaced by S_{z_r} and β_{z_r}, respectively.

For the second-order moments, one has

$$E\{|\hat{g}_2|^2\} = \frac{a^2}{\eta\frac{K_1}{K}} \frac{1-\rho}{\rho} E\{r_{z_r}^4\} E\left\{\frac{1}{r_{z_s}^2}\right\} \tag{4.93}$$

and

$$E\{|\hat{h}_2|^2\} = \frac{1}{(1-\rho)P_s a^2} E\{r_{z_s}^2\} E\left\{\frac{1}{r_{z_r}^2}\right\} \tag{4.94}$$

where $E\{r_{z_r}^4\}$, $E\{\frac{1}{r_{z_s}^2}\}$, $E\{r_{z_s}^2\}$, and $E\{\frac{1}{r_{z_r}^2}\}$ are derived by replacing S_{y_r}, β_{y_r}, S_{y_s}, and β_{y_s} with S_{z_r}, β_{z_r}, S_{z_s}, and β_{z_s} in the results for Scheme 1.

4.4.1.3 Scheme 3

In Scheme 1 and Scheme 2, channel estimation is only performed at the destination node by using pilots forwarded from the source node that contain the cascaded channel coefficient $|h|gh$ as well as pilots of the relay node's own that contain $|h|g$. This reduces the complexity at the relay node. The accuracy of channel estimation can be further improved if the relay node performs channel estimation. This is the case, for example, in variable-gain relaying.

In Scheme 3, the source node sends J_1 pilots to the relay node and the relay node uses these pilots to estimate the source-to-relay link h. Then, the source node sends I pilots to the relay node for energy harvesting. Using the harvested energy, the relay node sends J_2 pilots of its own to the destination node to estimate the relay-to-destination link g.

First, the source node sends J_1 pilots to the relay node such that the received signal at the relay node is

$$u_{r-ce}^{(j_1)} = \sqrt{P_s}h + n_{r-ce}^{(j_1)} \tag{4.95}$$

where $j_1 = 1, 2, \cdots, J_1$ and $n_{r-ce}^{(j_1)}$ is the AWGN with mean zero and variance $2\sigma^2$. Using (4.95), the relay node can estimate h as

$$E\{u_{r-ce}^{(j_1)}\} = \sqrt{P_s}h. \tag{4.96}$$

Secondly, the source node sends I pilots to the relay node for energy harvesting. The harvested energy is given by

$$E_h = \eta P_s |h|^2 I T_p. \tag{4.97}$$

Finally, the relay node uses the harvested energy to transmit J_2 pilots of its own to the destination node. The received signal at the destination is

$$u_{d-r}^{(j_2)} = \sqrt{P_r} g + n_{d-r}^{(j_2)} \tag{4.98}$$

where $j_2 = 1, 2, \cdots, J_2$. Since the harvested energy is used to transmit J_2 pilots, the transmission power of the relay is

$$P_r = \frac{E_h}{J_2 T_p} = \eta P_s |h|^2 \frac{I}{J_2}. \tag{4.99}$$

Using (4.99) in (4.98), one has

$$u_{d-r}^{(j_2)} = \sqrt{\eta P_s \frac{I}{J_2}} |h| g + n_{d-r}^{(j_2)}. \tag{4.100}$$

Thus,

$$E\{u_{d-r}^{(j_2)}\} = \sqrt{\eta P_s \frac{I}{J_2}} |h| g. \tag{4.101}$$

Using (4.96) and (4.101), the pilot-based MB estimators for g and h can be readily derived as

$$\hat{g}_3 = \frac{\frac{1}{J_2} \sum_{j_2=1}^{J_2} u_{d-r}^{(j_2)}}{\sqrt{\eta \frac{I}{J_2}} |\frac{1}{J_1} \sum_{j_1=1}^{J_1} u_{r-ce}^{(j_1)}|} \tag{4.102}$$

and

$$\hat{h}_3 = \frac{1}{\sqrt{P_s}} \frac{1}{J_1} \sum_{j_1=1}^{J_1} u_{r-ce}^{(j_1)}. \tag{4.103}$$

In Scheme 3, the relay node performs channel estimation of h and the estimate of h will be sent to the destination node via control channels for the estimation of g at the destination node. Thus, this scheme is more complicated than Scheme 1 and Scheme 2.

The first- and second-order moments can also be derived. We denote $u_r = \frac{1}{J_2} \sum_{j_2=1}^{J_2} u_{d-r}^{(j_2)} = r_{u_r} e^{j\theta_{u_r}}$ and $u_s = \frac{1}{J_1} \sum_{j_1=1}^{J_1} u_{r-ce}^{(j_1)} = r_{u_s} e^{j\theta_{u_s}}$. Then, u_r and u_s are complex Gaussian random variables with means $S_{u_r} = \sqrt{\eta P_s \frac{I}{J_2}} |h| g$ and $S_{u_s} = \sqrt{P_s} h$ and variances $2\beta_{u_r}^2 = \frac{2\sigma^2}{J_2}$ and $2\beta_{u_s}^2 = \frac{2\sigma^2}{J_1}$, respectively.

In this case, the first-order moment of $\hat{g}_3$ is given by

$$E\{\hat{g}_3\} = \sqrt{P_s} |h| g E\left\{ \frac{1}{r_{u_s}} \right\} \tag{4.104}$$

where $E\{\frac{1}{r_{u_s}}\}$ can be obtained by replacing S_{y_s} and β_{y_s} with S_{u_s} and β_{u_s}. It is also quite obvious that the first-order moment of $\hat{h}_3$ is

$$E\{\hat{h}_3\} = h \tag{4.105}$$

so that $\hat{h}_3$ is an unbiased estimator.

For the second-order moments, one has

$$E\{|\hat{g}_3|^2\} = \frac{J_2}{\eta I} E\{r_{u_r}^2\} E\left\{\frac{1}{r_{u_s}^2}\right\} \tag{4.106}$$

with $E\{r_{u_r}^2\} = 2\beta_{u_r}^2 + |S_{u_r}|^2$ and $E\{\frac{1}{r_{u_s}^2}\}$ are obtained by replacing S_{y_s} and β_{y_s} with S_{u_s} and β_{u_s}, respectively. Similarly, one has

$$E\{|\hat{h}_3|^2\} = \frac{2\sigma^2}{P_s J_1} + |h|^2. \tag{4.107}$$

4.4.1.4 Scheme 4

Scheme 4 is similar to Scheme 3, where the relay node estimates the source-to-relay link and the destination node estimates the relay-to-destination link, except that the relay node uses power splitting to harvest energy from the pilots sent by the source node that are also used for channel estimation at the relay node.

In this scheme, the source node sends K_1 pilots to the relay node, part of which is received for channel estimation as

$$v_{r-ce}^{(k_1)} = \sqrt{(1-\rho)P_s}h + n_{r-ce}^{(k_1)} \tag{4.108}$$

for $k_1 = 1, 2, \cdots, K_1$ and part of which is harvested with the harvested energy given by

$$E_h = \eta\rho P_s |h|^2 K_1 T_p. \tag{4.109}$$

The relay node uses (4.108) to estimate the source-to-relay link h as

$$E\{v_{r-ce}^{(k_1)}\} = \sqrt{(1-\rho)P_s}h. \tag{4.110}$$

Next, the relay node uses the harvested energy in (4.109) to transmit K_2 pilots of its own such that the received signal at the destination is

$$v_{d-r}^{(k_2)} = \sqrt{P_r}g + n_{d-r}^{(k_2)} \tag{4.111}$$

for $k_2 = 1, 2, \cdots, K_2$, where the transmission power is given by

$$P_r = \frac{E_h}{K_2 T_p} = \eta\rho P_s |h|^2 \frac{K_1}{K_2}. \tag{4.112}$$

Thus,

$$E\{v_{d-r}^{(k_2)}\} = \sqrt{\eta\rho P_s \frac{K_1}{K_2}}|h|g. \tag{4.113}$$

Using (4.110) and (4.113), the MB estimators for g and h can be derived, respectively, as

$$\hat{g}_4 = \frac{\frac{1}{K_2}\sum_{k_2=1}^{K_2} v_{d-r}^{(k_2)}}{\sqrt{\eta\frac{K_1}{K_2}\frac{\rho}{1-\rho}}|\frac{1}{K_1}\sum_{k_1=1}^{K_1} v_{r-ce}^{(k_1)}|} \tag{4.114}$$

and

$$\hat{h}_4 = \frac{1}{\sqrt{(1-\rho)P_s}}\frac{1}{K_1}\sum_{k_1=1}^{K_1} v_{r-ce}^{(k_1)}. \tag{4.115}$$

This scheme also requires channel estimation at both the relay and the destination.

In Scheme 4, let $v_r = \frac{1}{K_2}\sum_{k_2=1}^{K_2} v_{d-r}^{(k_2)} = r_{v_r}e^{j\theta_{v_r}}$ and $v_s = \frac{1}{K_1}\sum_{k_1=1}^{K_1} v_{r-ce}^{(k_1)} = r_{v_s}e^{j\theta_{v_s}}$ so that v_r is a complex Gaussian random variable with mean $S_{v_r} = \sqrt{\eta\rho P_s \frac{K_1}{K_2}}|h|g$ and variance $2\beta_{v_r}^2 = \frac{2\sigma^2}{K_2}$, and v_s is a complex Gaussian random variable with mean $S_{v_s} = \sqrt{(1-\rho)P_s}h$ and variance $2\beta_{v_s}^2 = \frac{2\sigma^2}{K_1}$.

Then, following similar procedures, one has

$$E\{\hat{g}_4\} = \sqrt{(1-\rho)P_s}|h|gE\left\{\frac{1}{r_{v_s}}\right\}, \tag{4.116}$$

$$E\{\hat{h}_4\} = h, \tag{4.117}$$

$$E\{|\hat{g}_4|^2\} = \frac{2\sigma^2 + \eta K_1\rho P_s|h|^2|g|^2}{\eta K_1\rho/(1-\rho)}E\left\{\frac{1}{r_{v_s}^2}\right\}, \tag{4.118}$$

$$E\{|\hat{h}_4|^2\} = \frac{2\sigma^2}{(1-\rho)P_sK_1} + |h|^2, \tag{4.119}$$

where $E\{\frac{1}{r_{v_s}}\}$ and $E\{\frac{1}{r_{v_s}^2}\}$ are obtained by replacing S_{y_s} and β_{y_s} with S_{v_s} and β_{v_s} in $E\{\frac{1}{r_{y_s}}\}$ and $E\{\frac{1}{r_{y_s}^2}\}$, respectively.

4.4.1.5 Scheme 5

In Scheme 5, the relay node does not send any pilots of its own. Instead, the relay node uses the pilots from the source node to estimate the source-to-relay link and the destination node uses the same pilots forwarded by the relay to estimate the relay-to-destination link. In contrast, in Scheme 1 and Scheme 2, the destination node uses the pilots from the relay node to estimate the relay-to-destination link and uses the pilots forwarded from the source node to estimate the source-to-relay link, while in Scheme 3 and Scheme 4 the relay node uses pilots from the source node to estimate the source-to-relay link and the destination node uses pilots from the relay node to estimate the relay-to-destination link.

First, I pilots are sent from the source node to the relay node for energy harvesting. Using time switching, the received signal at the relay node is given by (4.54). Thus, the harvested energy is the same as before.

Secondly, J pilots are sent from the source to the relay node for channel estimation. The received signal at the relay node is

$$w_{r-ce}^{(j)} = \sqrt{P_s}h + n_{r-ce}^{(j)} \tag{4.120}$$

where $j = 1, 2, \cdots, J$ and $n_{r-ce}^{(j)}$ is the complex AWGN with mean zero and variance $2\sigma^2$. This received signal is first used for channel estimation at the relay to give

$$E\{w_{r-ce}^{(j)}\} = \sqrt{P_s}h. \tag{4.121}$$

Then, the signal in (4.120) is forwarded by the relay node using the harvested energy as

$$w_{d-r}^{(j)} = \sqrt{P_r}gaw_{r-ce}^{(j)} + n_{d-r}^{(j)} \tag{4.122}$$

where the transmission power can be derived as $P_r = \frac{E_h}{JT_p} = \eta P_s |h|^2 \frac{I}{J}$. Thus, one has from (4.122)

$$E\{w_{d-r}^{(j)}\} = \sqrt{\eta \frac{I}{J}} P_s |h| g h a. \tag{4.123}$$

The MB estimators for g and h can be derived as

$$\hat{g}_5 = \frac{\frac{1}{J}\sum_{j=1}^{J} w_{d-r}^{(j)} \frac{1}{J}\sum_{j=1}^{J} w_{r-ce}^{(j)} *}{\sqrt{\eta \frac{I}{J}} a |\frac{1}{J}\sum_{j=1}^{J} w_{r-ce}^{(j)}|^3} \tag{4.124}$$

and

$$\hat{h}_5 = \frac{1}{\sqrt{P_s}} \frac{1}{J} \sum_{j=1}^{J} w_{r-ce}^{(j)}, \tag{4.125}$$

respectively. Note that $I + J = K$ for this scheme.

In this case, denote $w_r = \frac{1}{J}\sum_{j=1}^{J} w_{r-ce}^{(j)} = r_{w_r} e^{j\theta_{w_r}}$, which is a complex Gaussian random variable with mean $S_{w_r} = \sqrt{P_s} h$ and variance $2\beta_{w_r}^2 = \frac{2\sigma^2}{J}$.

For $\hat{g}_5$, one can first find the conditional moment, conditioned on w_r, and then take the expectation over w_r to have

$$E\{\hat{g}_5\} = \sqrt{P_s} |h| g E\left\{\frac{1}{r_{w_r}}\right\} \tag{4.126}$$

and

$$E\{|\hat{g}_5|^2\} = P_s |h|^2 |g|^2 E\left\{\frac{1}{r_{w_r}^2}\right\} + \frac{2\sigma^2}{\eta I a^2} E\left\{\frac{1}{r_{w_r}^4}\right\} \tag{4.127}$$

where $E\{\frac{1}{r_{w_r}}\}$ and $E\{\frac{1}{r_{w_r}^2}\}$ are obtained by replacing S_{y_s} and β_{y_s} with S_{w_r} and β_{w_r} in $E\{\frac{1}{r_{y_s}}\}$ and $E\{\frac{1}{r_{y_s}^2}\}$, respectively, and

$$E\{\frac{1}{r_{w_r}^4}\} = \int_0^\infty \frac{1}{\beta_{w_r}^2 x^3} e^{-\frac{x^2 + |S_{w_r}|^2}{2\beta_{w_r}^2}} I_0\left(\frac{x|S_{w_r}|}{\beta_{w_r}^2}\right) dx. \tag{4.128}$$

For $\hat{h}_5$, one also has

$$E\{\hat{h}_5\} = h \tag{4.129}$$

and

$$E\{|\hat{h}_5|^2\} = \frac{2\sigma^2}{P_s J} + |h|^2. \tag{4.130}$$

4.4.1.6 Scheme 6

In Scheme 6, power splitting is used to harvest the energy. The rest is similar to Scheme 5. In this case, the source node sends K pilots to the relay node, part of which is used for channel estimation at the relay node to estimate the source-to-relay link, giving

$$x_{r-ce}^{(k)} = \sqrt{(1-\rho)P_s} h + n_{r-ce}^{(k)} \tag{4.131}$$

where $k = 1, 2, \cdots, K$ and $n_{r-ce}^{(k)}$ is the complex AWGN with mean zero and variance $2\sigma^2$. The other part of the received power is used for energy harvesting with the harvested energy being

$$E_h = \eta\rho P_s |h|^2 K T_p. \tag{4.132}$$

Using (4.131), the source-to-relay link can be estimated as

$$E\{x_{r-ce}^{(k)}\} = \sqrt{(1-\rho)P_s}h. \tag{4.133}$$

The received signal in (4.131) is then forwarded to the destination using the harvested energy, giving

$$x_{d-r}^{(k)} = \sqrt{\eta\rho(1-\rho)}P_s|h|gha + \sqrt{\eta\rho P_s}|h|gan_{r-ce}^{(k)} + n_{d-r}^{(k)} \tag{4.134}$$

where $n_{d-r}^{(k)}$ is also AWGN with mean zero and variance $2\sigma^2$. Thus,

$$E\{x_{d-r}^{(k)}\} = \sqrt{\eta\rho(1-\rho)}P_s|h|gha. \tag{4.135}$$

Finally, one has

$$\hat{g}_6 = \frac{\frac{1}{K}\sum_{k=1}^{K} x_{d-r}^{(k)} \frac{1}{K}\sum_{k=1}^{K} x_{r-ce}^{(k)*}}{a\sqrt{\eta\frac{\rho}{1-\rho}}|\frac{1}{K}\sum_{k=1}^{K} x_{r-ce}^{(k)}|^3} \tag{4.136}$$

$$\hat{h}_6 = \frac{1}{\sqrt{(1-\rho)P_s}}\frac{1}{K}\sum_{k=1}^{K} x_{r-ce}^{(k)}. \tag{4.137}$$

The derivation in Scheme 6 is very similar to that in Scheme 5. Let $x_r = \frac{1}{K}\sum_{k=1}^{K} x_{r-ce}^{(k)} = r_{x_r}e^{j\theta_{x_r}}$, which is a complex Gaussian random variable with mean $S_{x_r} = \sqrt{(1-\rho)P_s}h$ and variance $2\beta_{x_r}^2 = \frac{2\sigma^2}{K}$.

For $\hat{g}_6$, one can also first find the conditional moment, conditioned on x_r, and then take the expectation over x_r to have

$$E\{\hat{g}_6\} = \sqrt{(1-\rho)P_s}|h|gE\left\{\frac{1}{r_{x_r}}\right\} \tag{4.138}$$

and

$$E\{|\hat{g}_6|^2\} = (1-\rho)P_s|h|^2|g|^2E\left\{\frac{1}{r_{x_r}^2}\right\} + \frac{2\sigma^2}{\eta K a^2\rho/(1-\rho)}E\left\{\frac{1}{r_{x_r}^4}\right\} \tag{4.139}$$

where $E\{\frac{1}{r_{x_r}}\}$ and $E\{\frac{1}{r_{x_r}^2}\}$ are obtained by replacing S_{y_s} and β_{y_s} with S_{x_r} and β_{x_r} in $E\{\frac{1}{r_{y_s}}\}$ and $E\{\frac{1}{r_{y_s}^2}\}$, respectively, and

$$E\left\{\frac{1}{r_{x_r}^4}\right\} = \int_0^\infty \frac{1}{\beta_{x_r}^2 x^3} e^{-\frac{x^2+|S_{x_r}|^2}{2\beta_{x_r}^2}} I_0\left(\frac{x|S_{x_r}|}{\beta_{x_r}^2}\right)dx. \tag{4.140}$$

For $\hat{h}_6$, its first-order moment and second-order moment are given by

$$E\{\hat{h}_6\} = h \tag{4.141}$$

and

$$E\{|\hat{h}_6|^2\} = \frac{2\sigma^2}{(1-\rho)P_s K} + |h|^2, \tag{4.142}$$

respectively.

Next, we use some graphs to show the performances of the obtained estimators for h and g in terms of the MSE. From the first- and second-order moments of the estimates, one can see that the estimator performance depends on various system parameters, including η, P_s, $2\sigma^2$, g, h, K, I and J. For η, P_s, $2\sigma^2$, and K, their effects on the estimator performance are quite straightforward. In particular, it is expected that the estimator performance improves when η, P_s, and K increase or when $2\sigma^2$ decreases, as this reduces the noise which is the main source of estimation error. Thus, in the examination, we set $\eta = 0.5$, $P_s = 1$, $K = 100$, and $2\sigma^2 = 2$ to focus on the effects of g, h, I, J_2, ρ, K_1, and K_2. Define $\gamma_g = \frac{|g|^2}{2\sigma^2}$ as the instantaneous SNR of the relay-to-destination link and $\gamma_h = \frac{|h|^2}{2\sigma^2}$ as the instantaneous SNR of the source-to-relay link. The values of g and h will change with γ_g and γ_h and their real and imaginary parts are equal to each other. The MSE is defined as $\frac{1}{R}\sum_{r=1}^{R}|g-\hat{g}_r|^2$, $\frac{1}{R}\sum_{r=1}^{R}|h-\hat{h}_r|^2$, and $\frac{1}{R}\sum_{r=1}^{R}|gh-\hat{g}_r\hat{h}_r|^2$ for $\hat{g}$, $\hat{h}$, and $\hat{g}\hat{h}$, respectively, where $R = 10\,000$ is the total number of simulation runs and $\hat{g}_r$ and $\hat{h}_r$ are the channel estimates in the rth run.

Figures 4.15 and 4.16 show the MSE of the estimators $\hat{g}_1$ and $\hat{h}_1$ in Scheme 1 versus the values of I and J_2, respectively, when different values of SNR or different values of g and h are considered. In Figure 4.15, the values of J_1 and J_2 are set as $\frac{J}{2}$ to focus on the effect of I, and the value of I is examined from 4 to 96 with a step size of 4. In Figure 4.16, the values of I are fixed to focus on the effect of J_2, and the value of J_2 is examined from 2 to $J-2$ with a step size of 2. Several observations can be made. First, from Figure 4.15, the

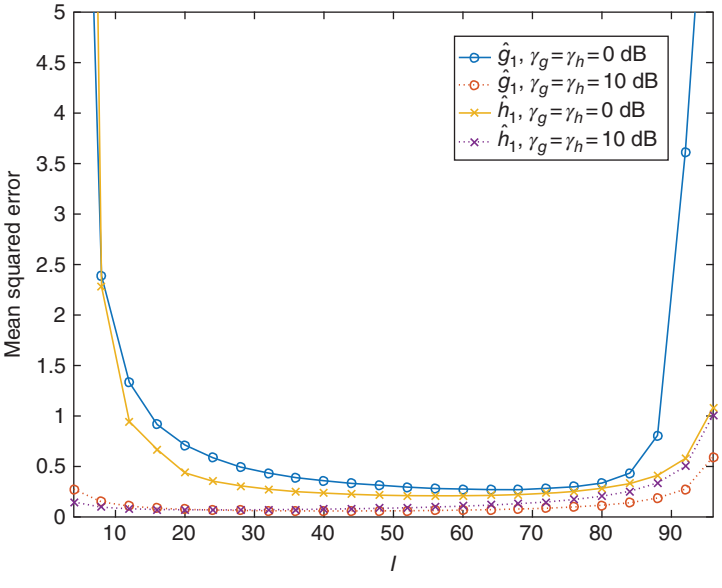

Figure 4.15 MSE of $\hat{g}_1$ and $\hat{h}_1$ versus I for different values of SNR in Scheme 1.

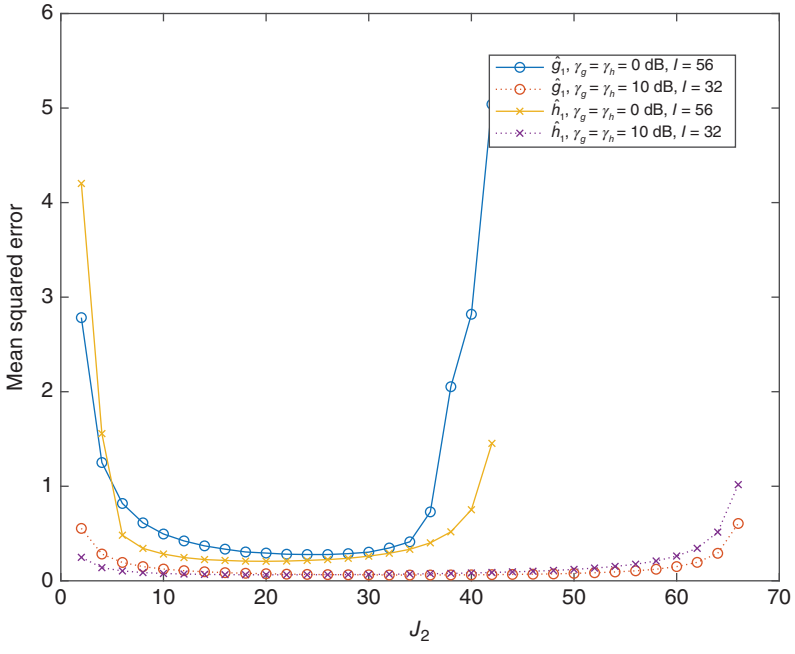

Figure 4.16 MSE of $\hat{g}_1$ and $\hat{h}_1$ versus J_2 for different values of SNR in Scheme 1.

MSE first decreases and then increases with the value of I, as expected, as a larger value of I leads to more harvested energy such that the estimation at the destination node will be more accurate but it also leads to a smaller value of J due to fixed K such that the sample size in the estimation reduces. The optimum value of I exists, and there is also a wide range of choices for I that give close-to-optimum performances. This provides flexibility in system design. Secondly, under the same conditions, the estimator generally performs better with a larger value of SNR, as expected, as a larger SNR gives relatively smaller noise, which is the main source of estimation error. Also, the performance of $\hat{g}_1$ is close to that of $\hat{h}_1$, especially near the optimum values of I. Finally, from Figure 4.16, the MSE first decreases and then increases when the value of J_2 increases. This is also expected. A larger value of J_2 leads to a better approximation of $E\{y_{d-r}^{(j_2)}\}$ but due to fixed J it also leads to a worse approximation of $E\{y_{d-s}^{(j_1)}\}$. Since both of them are needed in $\hat{g}_1$ and $\hat{h}_1$, their interaction yields an optimum value of J_2, as seen from Figure 4.16.

Figures 4.17 and 4.18 show the MSE versus ρ and K_2, respectively, for $\hat{g}_2$ and $\hat{h}_2$ in Scheme 2. In Figure 4.17, the value of ρ is examined from 0.1 to 0.9 with a step size of 0.1, when $K_2 = \frac{K}{2}$ is fixed to focus on the effect of ρ. In Figure 4.18, the value of K_2 is examined from 4 to 96 with a step size of 4, while the value of ρ is fixed. Again, optimum values of ρ and K_2 exist. For ρ, when it is large, more energy is harvested for relay transmission but the signal component in the samples will be weaker, leading to more estimation errors. Thus, a balanced choice of ρ needs to be made and it plays a similar role to $\frac{I}{K}$ in Scheme 1. From Figure 4.17, the MSE curve is relatively flat between 0.2 and 0.8, indicating that there is a wide range of choices for ρ that can achieve close-to-optimum performance, which is desirable for system design. For K_2, since K is fixed, a larger value

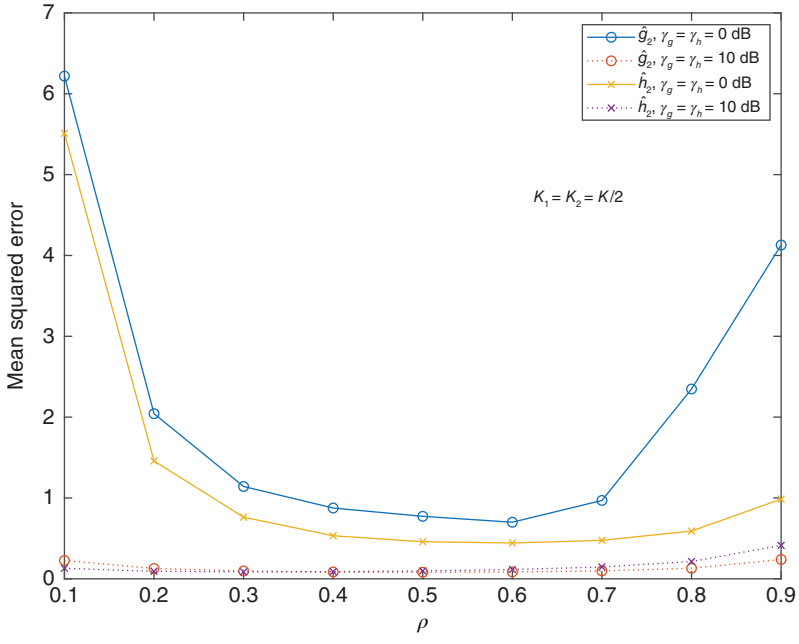

Figure 4.17 MSE of $\hat{g}_2$ and $\hat{h}_2$ versus ρ for different values of SNR in Scheme 2.

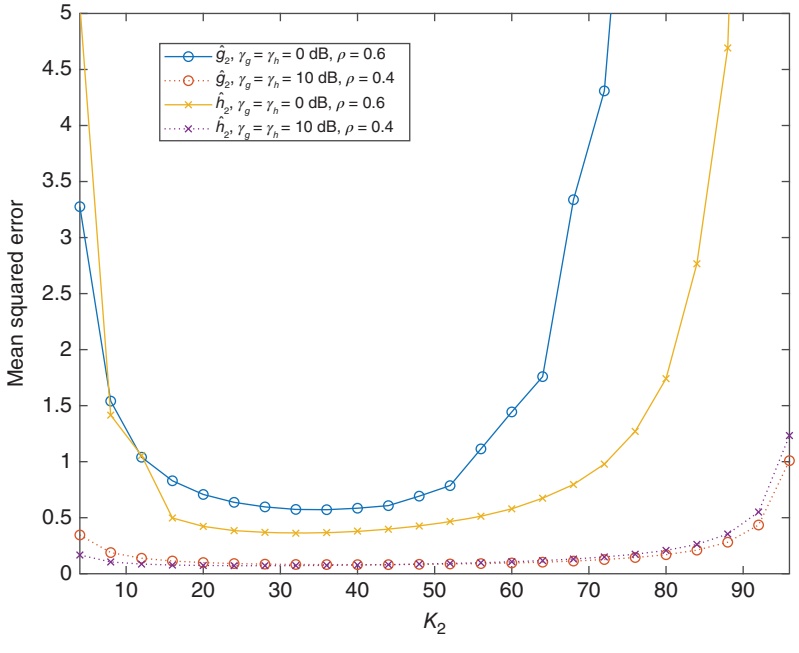

Figure 4.18 MSE of $\hat{g}_2$ and $\hat{h}_2$ versus K_2 for different values of SNR in Scheme 2.

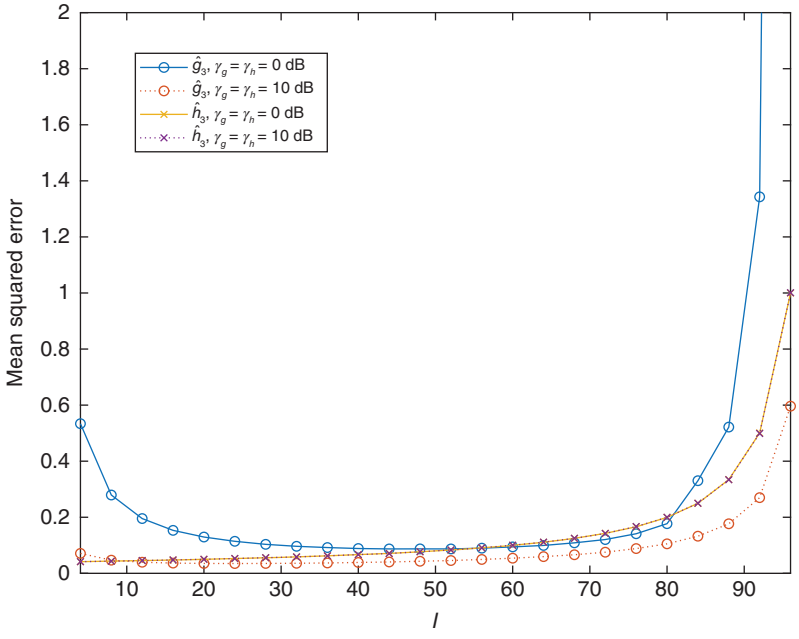

Figure 4.19 MSE of $\hat{g}_3$ and $\hat{h}_3$ versus I for different values of SNR in Scheme 3.

of K_2 gives a better approximation using the pilots from the relay node but also gives a worse approximation using the pilots from the source node, as K_1 will be smaller. In all cases, increasing the SNR reduces the MSE.

Figures 4.19 and 4.20 show the MSE versus I and J_1, respectively, for $\hat{g}_3$ and $\hat{h}_3$ in Scheme 3. In Figure 4.19, the value of I is examined from 4 to 96 with a step size of 4, when $J_1 = \frac{J}{2}$ is fixed to focus on the effect of I. Also, in Figure 4.20, the value of J_1 is examined from 2 to $J-2$ with a step size of 2, while the value of ρ in this figure is fixed. In Figure 4.19, the optimum value of I still exists for $\hat{g}_3$, as the value of I affects both energy harvesting and the sample size for $\hat{g}_3$. However, for $\hat{h}_3$, its MSE monotonically increases with I, as the estimation of h does not rely on energy harvesting and it only relies on J_1. When I increases, for fixed K, the value of J_1 decreases such that more estimation errors occur. Also in this case, the SNR has very minor effect on $\hat{h}_3$. In Figure 4.20, it can also be seen that the optimum value of J_1 does not exist.

Figures 4.21 and 4.22 show the MSE versus ρ and K_1, respectively, for $\hat{g}_4$ and $\hat{h}_4$ in Scheme 4. In Figure 4.21, the value of ρ is studied from 0.1 to 0.9 with a step size of 0.1, while we fix $K_1 = \frac{K}{2}$ to focus on the effect of ρ. As well, in Figure 4.22, the value of K_1 is examined from 4 to 96 with a step size of 4, while the value of ρ in this figure is fixed. As can be seen from Figure 4.21, the value of ρ affects the performance of $\hat{g}_4$ both ways, making its MSE larger due to weaker signal component in the samples and less accurate $\hat{h}_4$ but also making its MSE smaller due to more harvested energy, when ρ increases. For $\hat{h}_4$, increasing ρ will increase the MSE of $\hat{h}_4$ as the signal component in $v_{r-ce}^{(k_1)}$ will be weaker. Also, similar to Figure 4.20, increasing K_1 reduces the MSE of the estimator.

For Scheme 5 and Scheme 6, the effects of the system parameters are straightforward. From their expressions of the first- and second-order moments, it can be expected that

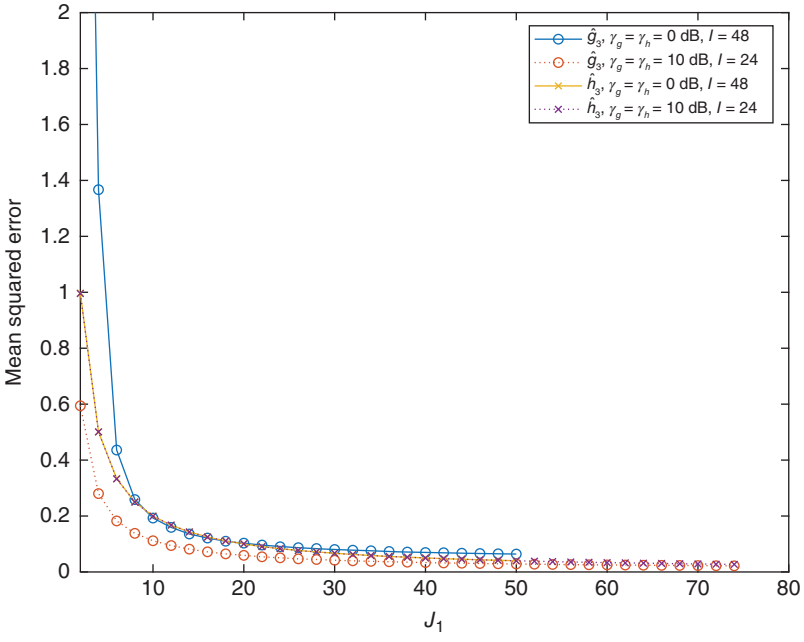

Figure 4.20 MSE of $\hat{g}_3$ and $\hat{h}_3$ versus J_1 for different values of SNR in Scheme 3.

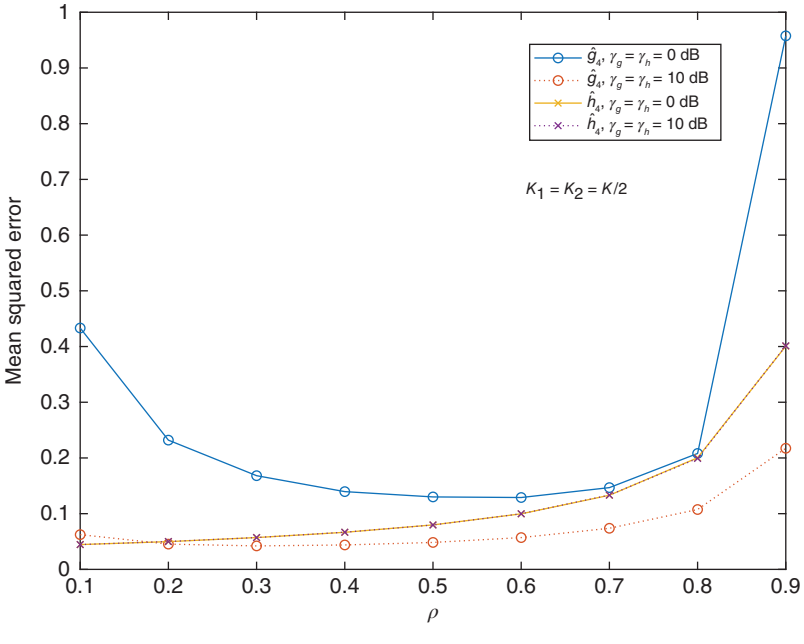

Figure 4.21 MSE of $\hat{g}_4$ and $\hat{h}_4$ versus ρ for different values of SNR in Scheme 4.

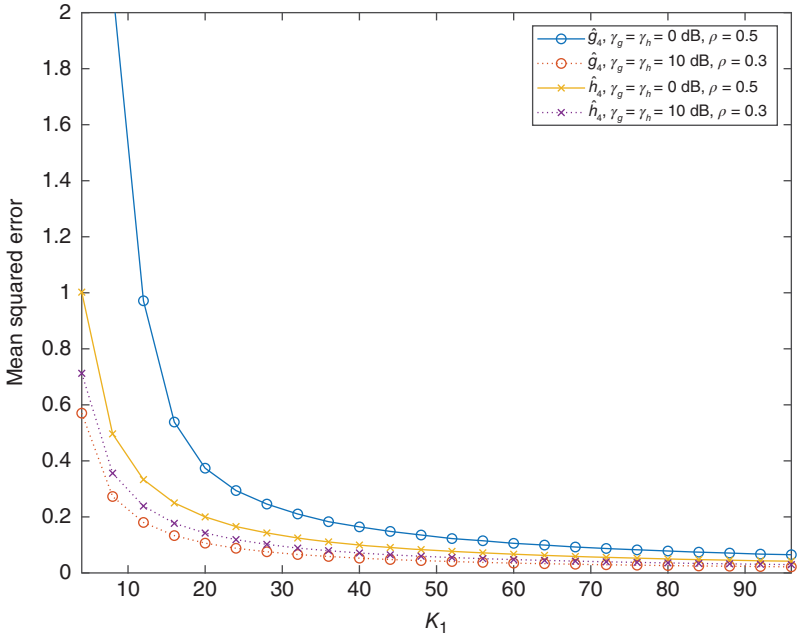

Figure 4.22 MSE of $\hat{g}_4$ and $\hat{h}_4$ versus K_1 for different values of SNR in Scheme 4.

the MSE of $\hat{h}_5$ increases when I increases and for the MSE of $\hat{g}_5$ there is an optimum I due to the interaction between energy harvesting and sample size. Also, the MSE of $\hat{h}_6$ monotonically increases when ρ increases due to weaker signal component in the samples, while the MSE of $\hat{g}_6$ first decreases then increases with ρ. They are not shown here.

Figures 4.23 and 4.24 compare the estimators in different schemes in terms of their minimum MSE of $\hat{g}\hat{h}$ achieved by performing exhaustive searches over the relevant parameters. One sees from these two figures that Scheme 5 and Scheme 6 have the best performances, followed by Scheme 3 and Scheme 4, and Scheme 1 and Scheme 2 have the worst performance. Also, Scheme 5 outperforms Scheme 6, Scheme 3 outperforms Scheme 4, and Scheme 1 outperforms Scheme 2, indicating that time switching leads to better MSE performance than power splitting. Finally, the estimator performance is more sensitive to γ_g than to γ_h. More details of derivations can be found in Chen et al. (2017b).

4.4.2 Without Relaying

In this subsection, we consider the case without relaying. In this case, the transmission contains three parts: channel estimation; energy harvesting; and data transmission. Figure 4.25 shows a diagram of the considered data frame. In this system, the data frame is first divided into two parts in time for channel estimation and data transmission. Then, each part in time is divided into two parts in amplitude so that energy harvesting is performed by taking parts of the received energy for channel estimation as well as parts of the received energy for data transmission. This is equivalent to dividing the whole data

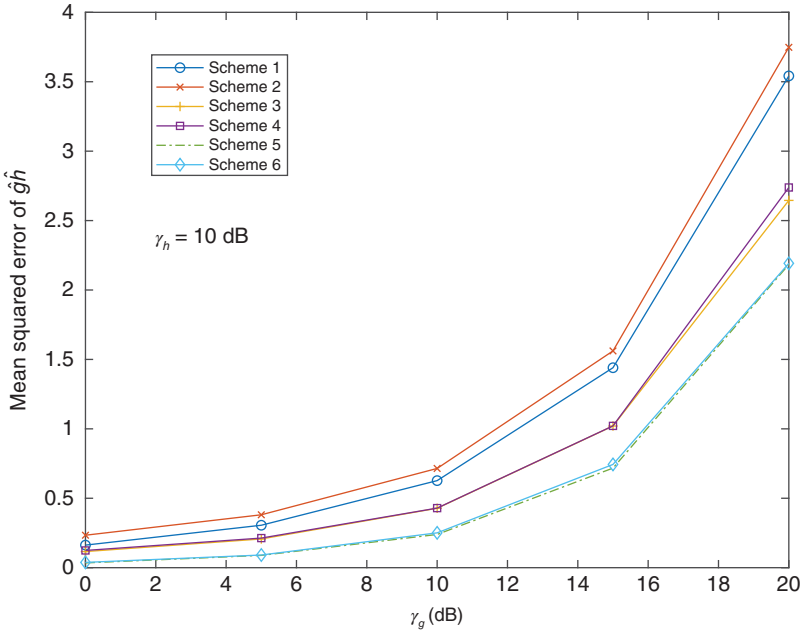

Figure 4.23 MSE of $\hat{gh}$ versus γ_g for different schemes.

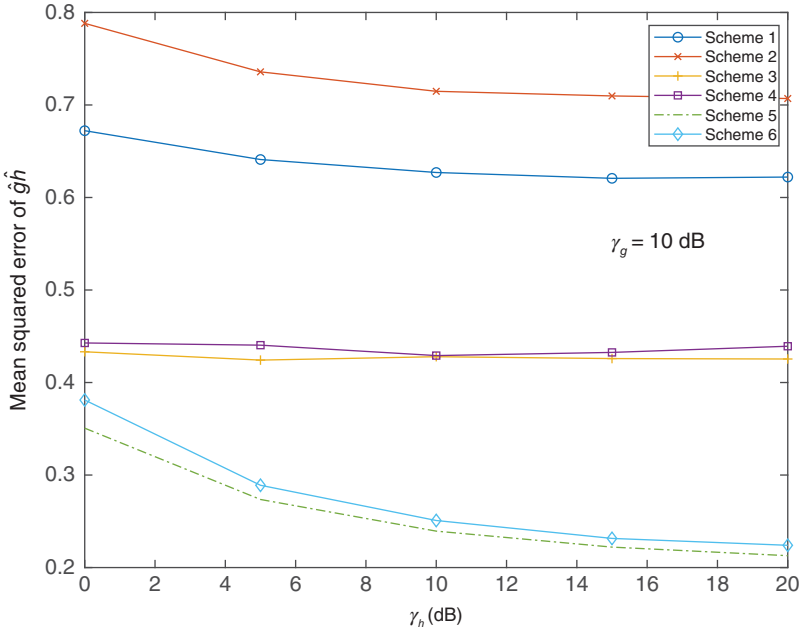

Figure 4.24 MSE of $\hat{gh}$ versus γ_h for different schemes.

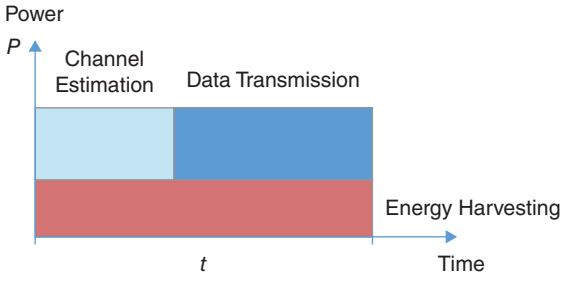

Figure 4.25 The considered data frame with three parts.

frame into three parts in time only. It is the area of the block in the figure that matters, as it represents the energy allocation.

From this diagram, the received signals for the pilots used in channel estimation can be expressed as

$$p_i = \sqrt{\rho_p P_s} h + n_i \tag{4.143}$$

where $i = 1, 2, \cdots, L$ index the pilots, P_s is the transmission power, ρ_p is the portion of power split from the received signal for channel estimation, h is the complex fading gain to be estimated, and n_i is the complex AWGN with mean zero and variance $2\sigma^2$. These pilots can be used to estimate the channel gain using the maximum likelihood method as

$$\hat{h} = \frac{1}{\sqrt{\rho_p P_s} L} \sum_{i=1}^{L} p_i = h + e \tag{4.144}$$

where the estimation error e is Gaussian with mean zero and variance $\frac{2\sigma^2}{\rho_p P_s L}$.

The received signals of the symbols used for information delivery can be expressed as

$$y_i = \sqrt{\rho_d P_s} h + n_i \tag{4.145}$$

where $i = L+1, L+2, \cdots, L+M$ index the data symbols to be decoded and ρ_d is the portion of power split from the received signal for data decoding. Using the estimate in (4.144), one has

$$y_i = \sqrt{\rho_d P_s} \hat{h} - \sqrt{\rho_d P_s} e + n_i. \tag{4.146}$$

Thus, the achievable rate can be derived as

$$R = \frac{M}{L+M} \log_2 \left(1 + \frac{\rho_d P_s |\hat{h}|^2}{2\sigma^2 + \rho_d \frac{2\sigma^2}{\rho_p L}} \right). \tag{4.147}$$

Finally, the total energy harvested from pilots for channel estimation and symbols for information delivery can be derived as

$$E = \eta(1-\rho_p) P_s |h|^2 L + \eta(1-\rho_d) P_s |h|^2 M \tag{4.148}$$

where η is the conversion efficiency defined as before. The average energy harvested over each symbol is thus

$$\bar{E} = \frac{E}{L+M} = 2\alpha^2 \eta P_s \frac{(1-\rho_p)L + (1-\rho_d)M}{L+M} \tag{4.149}$$

where $E\{|h|^2\} = 2\alpha^2$ has been used.

From the above, the pilot symbols are used for channel estimation. The estimated channel gain is then used for data decoding. At the same time, both the pilot and data symbols are harvested for energy. Putting all these requirements together, we can formulate an optimization problem as

$$\max_{\rho_p, \rho_d, L} R \tag{4.150}$$

$$\text{subject to } \bar{E} \geq E_0 \tag{4.151}$$

$$1 \geq \rho_p \geq 0 \tag{4.152}$$

$$1 \geq \rho_d \geq 0 \tag{4.153}$$

$$M + L \geq L \geq 0. \tag{4.154}$$

In this problem, we try to maximize the average achievable rate for information delivery with respect to the number of pilots for channel estimation as well as the two power splitting parameters ρ_p and ρ_d, while satisfying a minimum requirement on the harvested energy per symbol. The values of L, ρ_p, and ρ_d actually determine the energy allocation between channel estimation, data transmission, and energy harvesting within the transmitted data frame. Thus, this is essentially a resource allocation problem. It is related to the second issue discussed at the beginning of this section, that is, the addition of energy harvesting capability consumes resources provided for other functions and therefore, it needs to be carefully chosen. A similar problem was studied in Zhou (2015), where a minimum mean squared error channel estimator was considered, but the rest of the settings are similar to those in this subsection. Also, without energy harvesting, the problem in (4.150) becomes the classical pilot allocation problem in conventional communications, where a larger number of pilots gives better estimation accuracy but reduces the throughput of the channel (Wang et al. 2014).

In the following, we consider a simpler case when $\rho_d = \rho_p = \rho$. Also, fix $L + M = K$ so that $M = K - L$. Using them in (4.148), the optimization problem becomes

$$\max_{\rho, L} \quad \frac{K-L}{K} \log_2 \left(1 + \frac{\rho P_s |\hat{h}|^2}{2\sigma^2 + \frac{2\sigma^2}{L}} \right) \tag{4.155}$$

$$\text{subject to} \quad 2\alpha^2 \eta (1-\rho) P_s K \geq E_0 \tag{4.156}$$

$$1 \geq \rho \geq 0 \tag{4.157}$$

$$K \geq L \geq 0. \tag{4.158}$$

One sees that the rate monotonically increases with ρ so that the optimum ρ is determined by the constraint on the harvested energy as $\rho_{opt} = \max\{0, 1 - \frac{E_0}{2\alpha^2 \eta P_s K}\}$. By replacing ρ with the optimum value in the rate expression, one has the rate as the function of a single variable L. By taking the first-order derivative of this function with respect to L and solving the equation for L, the optimum L can be obtained. This involves a non-linear function due to the logarithm function. We show some numerical results instead. Let $P_s = 1$, $|\hat{h}|^2 = 1$, $K = 100$, $2\sigma^2 = 1$, $\eta = 0.5$, $E_0 = 50$, and $2\alpha^2 = 1$. Figure 4.26 shows R versus L under these conditions using the optimum ρ. From this figure, the optimum L is around 8.

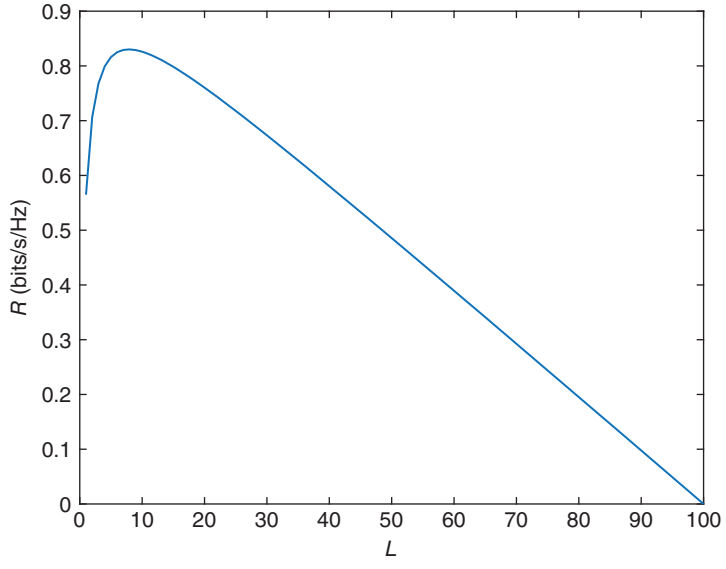

Figure 4.26 *R* versus *L*.

This problem has many variants that one can work on. For example, instead of using the instantaneous achievable rate, one may use the average achievable rate as the objective function. Thus, R will be replaced by $E_{\hat{h}}\{R\}$ in the above problems, where $E\{\cdot\}$ denotes the expectation operator. Also, one can consider the sum rate in the downlink and uplink. In this case, the uplink rate decreases with the parameter ρ due to a reduced harvested energy. Thus, the constraint on the harvested energy is not needed any more but the tradeoff will be reflected by the fact that the downlink rate increases with ρ while the uplink rate decreases with ρ.

The key point in these optimizations and in energy harvesting estimation generally is that both energy harvesting and channel estimation are part of the overhead incurred for data transmission. Hence, an increase in one part will lead to a decrease in the other part, assuming a fixed amount of resource. In Yang et al. (2014) and Zeng and Zhang (2015b), only channel estimation and energy harvesting were considered in the tradeoff, without taking into account the achievable rate for data transmission. One can either maximize the amount of harvested energy with respect to a constraint on the estimation accuracy or vice versa. Again, the fundamental problem in all these studies is the tradeoff between energy harvesting and channel estimation subject to limited resource. This is unique for energy harvesting estimation, as conventional communications do not have this allocation issue.

4.5 Energy Transmission Waveform

For information transmission, it is well known that the transmitted pulse can be optimized to achieve the largest signal-to-interference-plus-noise ratio for best

performance. Similarly, for power transfer, the transmitted waveform can also be optimized to achieve the maximum transferred power. In an energy harvesting communications system, this is part of the signal design problem at the transmitter.

The transferred power needs to be harvested and maximized at the receiver. Thus, the amount of transferred power is a function of the parameters of the transmitted waveform at the transmitter, the parameters of the communications channel, and the parameters of the energy harvester at the receiver. To optimize the transmitted waveform for maximum transferred power, one must know the channel parameters and the energy harvester parameters, as the optimal waveform will be adapted to the channel conditions and the harvester designs. Next, energy transfer waveform design will be discussed.

4.5.1 Scenario

Consider a wireless energy transfer system where there are M energy sources with $M > 1$. Each source transmits an energy waveform with a complex amplitude of $w_m = \omega_m e^{j\psi_m}$, where $m = 1, 2, \cdots, M$ index the sources, $j = \sqrt{-1}$, ω_m is the magnitude of the energy waveform, and ψ_m is the phase of the energy waveform. These ω_m and ψ_m are the parameters to be optimized. The waveforms are transmitted over Rayleigh fading channels. The faded signals are then harvested by the energy harvesters at the receiver. These M energy sources could be M simultaneously transmitting users. In this case, only one harvester is needed to harvest all energies. These M energy sources could also be M antennas, frequency bands or time slots. In this case, either M harvesters will be needed or the same harvester will be used for M times.

In the multi-user case, if all users transmit their waveforms simultaneously in the same frequency band using the same antenna, the received signal at the single harvester is

$$z = \sum_{m=1}^{M} w_m h_m + n \tag{4.159}$$

where h_m is the fading gain from the mth user to the energy harvester and n is the AWGN with mean zero and variance $2\sigma^2$. The channel gain h_m is a circularly symmetric complex Gaussian random variable with mean zero and variance $2\alpha_m^2$. For example, in a two-way relaying system or a non-orthogonal multiple access (NOMA) system, the received signals come from all users. Also, if co-channel interference is harvested, the received energy is made of signals from all interfering users too. Using (4.159), if a linear energy harvester is used, the harvested power (the term power is used interchangeably with the term energy here due to the fixed time slot) is

$$P_o = \eta |z|^2 \tag{4.160}$$

where η is the conversion efficiency of the harvester. Thus, the harvested power is a function of the waveform parameters ω_m and ψ_m, the channel parameters h_m, and the harvester parameter η, as mentioned before. If a non-linear energy harvester is used, as discussed in Chen et al. (2017d), the harvested power is

$$P_o = \frac{a|z|^2 + b}{|z|^2 + c} - \frac{b}{c} \tag{4.161}$$

where a, b, and c are the parameters of the harvester that can be determined by standard curve-fitting methods.

On the other hand, if the sources operate over different antennas, frequency bands, or time slots, one needs M energy harvesters, or one harvester used for M times. For the mth harvester, the received signal to be harvested is given by

$$z_m = w_m h_m + n_m \tag{4.162}$$

where n_m is the AWGN with mean zero and variance $2\sigma^2$, and all the other symbols are defined as before. This is, for example, the case when harvesters are tuned at different frequencies (Sun et al. 2013) or antennas (He et al. 2015) to increase the amount of harvested energy, or when the energy is accumulated from transmissions in different time slots. In this case, using the linear harvester, the total harvested energy is given by

$$P_o = \sum_{m=1}^{M} \eta_m |z_m|^2 \tag{4.163}$$

and using the non-linear harvester, the total harvested energy is

$$P_o = \sum_{m=1}^{M} \left(\frac{a_m |z_m|^2 + b_m}{|z_m|^2 + c_m} - \frac{b_m}{c_m} \right), \tag{4.164}$$

where η_m is the conversion efficiency of the mth harvester. In this case, the individual signals are harvested and combined.

4.5.2 Energy Waveform Optimization

Here we consider the optimization of the average total harvested power, subject to the constraint that the total transmitted power is fixed for all M sources. Thus, the optimization problem is written as

$$\{\hat{w}_1, \cdots, \hat{w}_M\} = \max_{w_1, \cdots, w_M} \{E\{P_o\}\}, \text{ with } \sum_{m=1}^{M} |w_m|^2 = P \tag{4.165}$$

where $E\{\cdot\}$ is the expectation operation and P is the total power limit. This optimization depends on the harvester model and the channel condition.

4.5.2.1 Linear Harvester

When a single linear energy harvester is used, the average harvested power can be calculated from (4.160) as

$$E\{P_o\} = \eta \left[\sum_{m=1}^{M} (2\alpha_m^2)\omega_m^2 + 2\eta\sigma^2 \right]. \tag{4.166}$$

This value can be easily maximized using linear programming to give the maximum average harvested power as

$$E\{P_o\}_{max} = 2\eta P \alpha_{\hat{m}}^2 + 2\sigma^2 \tag{4.167}$$

where $\hat{m} = \max_{m=1,2,\cdots,M} \{2\alpha_m^2\}$. Thus, the optimum waveforms are given by $\omega_m^2 = P$ when $m = \hat{m}$ and $\omega_m^2 = 0$ when $m \neq \hat{m}$. In other words, the maximum harvested power can be achieved by transmitting all the power P at the user with the highest average channel

fading power to the energy harvester and switch off all other users. In doing so, the phase of the optimum waveform can be an arbitrary value.

In the second case when multiple linear harvesters are used over different frequencies, antennas or time slots, similarly, the average total harvested power is calculated from (4.163) as

$$E\{P_o\} = 2\sum_{m=1}^{M} \eta_m \alpha_m^2 \omega_m^2 + 2\sum_{m=1}^{M} \eta_m \sigma^2. \tag{4.168}$$

Again, using linear programming, this value can be maximized as

$$E\{P_o\}_{max} = 2\eta_{\hat{m}} P \alpha_{\hat{m}}^2 + 2\sum_{m=1}^{M} \eta_m \sigma^2 \tag{4.169}$$

where $\hat{m} = \max_{m=1,2,\cdots,M} \{2\eta_m \alpha_m^2\}$ in this case and the optimum waveform is achieved by setting $\omega_m^2 = P$ when $m = \hat{m}$ and $\omega_m^2 = 0$ when $m \neq \hat{m}$.

4.5.2.2 Non-Linear Harvester

In many applications, the energy harvester is not linear. Consider the single harvester case first. In this case, the average harvested power can be derived from (4.161) by taking the expectation to give

$$E\{P_o\} = a - \frac{b}{c} + \frac{b-ac}{2\beta^2} e^{\frac{c}{2\beta^2}} \left[-Ei\left(-\frac{c}{2\beta^2}\right)\right] \tag{4.170}$$

where $2\beta^2 = 2\sum_{m=1}^{M} \omega_m^2 \alpha_m^2 + 2\sigma^2$ and $Ei(\cdot)$ represents the exponential integral Gradshteyn and Ryzhik (2000, eq. (8.211.1)). If one denotes $g(x) = xe^x[-Ei(-x)]$, one can show that $g(x)$ is a monotonically increasing function of x. Thus, the maximization of the average harvested power in (4.170) is equivalent to the maximization of $2\beta^2$ in that function. However, $2\beta^2$ is a quadratic form of ω_m. Thus, the maximum harvested power is

$$E\{P_o\}_{max} = a - \frac{b}{c} + \frac{b-ac}{2\hat{\beta}^2} e^{\frac{c}{2\hat{\beta}^2}} \left[-Ei\left(-\frac{c}{2\hat{\beta}^2}\right)\right] \tag{4.171}$$

where $2\hat{\beta}^2 = 2P\alpha_{\hat{m}}^2 + 2\sigma^2$ and $\hat{m} = \max_{m=1,2,\cdots,M} \{2\alpha_m^2\}$. The optimum waveforms are $\omega_m^2 = P$ when $m = \hat{m}$ and $\omega_m^2 = 0$ when $m \neq \hat{m}$. Again, in this case, one allocates the full power to the source with the best channel condition and switches off all other sources.

In the case when multiple non-linear harvesters are used, one can use the Lagrange multiplier to find the optimum solution. In this case, the function $g(x)$ defined before can be approximated as $g(x) \approx \frac{0.98x+0.12}{x+0.86}$ by curve-fitting for $0 < x < 30$. Then, one has the target function for optimization as

$$\sum_{m=1}^{M} \left(a_m - \frac{b_m}{c_m}\right) + \sum_{m=1}^{M} (b_m - a_m c_m) \frac{0.98c_m + 0.12(\omega_m^2 2\alpha_m^2 + 2\sigma^2)}{c_m + 0.86(\omega_m^2 2\alpha_m^2 + 2\sigma^2)} + \lambda\left(P - \sum_{m=1}^{M} \omega_m^2\right) \tag{4.172}$$

where λ is the Lagrange multiplier. Using (4.172), one has the optimum waveforms as

$$\omega_m^2 = \frac{\sqrt{1.2\alpha_m^2 c_m (a_m c_m - b_m)/\lambda_0} - c_m - 1.72\sigma^2}{1.72\alpha_m^2} \tag{4.173}$$

where $\lambda_0 = \left(\frac{\sum_{m=1}^{M} \frac{\sqrt{1.2a_m^2 c_m (a_m c_m - b_m)}}{1.72a_m^2}}{P + \sum_{m=1}^{M} \frac{c_m + 1.72\sigma^2}{1.72a_m^2}} \right)^2$. One sees that, in this case, the optimum waveforms are not to transmit the full power over the best channel any more. Instead, the power needs to be distributed among different frequencies, antennas, or time slots. In all the above cases, the phase of the optimum waveform can be arbitrary. This gives flexibility in the system design. More details on this work can be found in Chen et al. (2017d), where in addition to Rayleigh fading, the general Rician fading channel and the Gamma-shadowed Rician fading channel have also been discussed.

The above discussion considered the use of a single harvester for signals from multiple users or multiple time slots, or the use of multiple harvesters for signals from multiple antennas and frequencies. In Clerckx and Bayguzina (2016), the authors considered the other case when a single harvester is used for a sum of signals from multiple antennas and frequency bands and the noise can be ignored. Specifically, the received signal at the single harvester is given by Clerckx and Bayguzina (2016, eq. (4))

$$y = \Re \left\{ \sum_{n=1}^{N} \mathbf{h}_n \mathbf{w}_n e^{j2\pi f_n t} \right\} \tag{4.174}$$

where $\Re\{\cdot\}$ takes the real part of a complex value, $n = 1, 2, \cdots, N$ index N frequency bands or subcarriers within the signal bandwidth, f_n is the nth frequency band, $\mathbf{h}_n = [h_{n,1} h_{n,2} \cdots h_{n,M}]$ is the channel gain in the nth frequency for M transmitting antennas, and $\mathbf{w}_n = [w_{n,1} w_{n,2} \cdots w_{n,M}]^T$ is the waveform amplitude to be determined in the nth frequency band for M transmitting antennas, $(\cdot)^T$ is the transpose operation, N is the total number of frequencies, and M is the total number of antennas. Compared with (4.159), one can notice several differences. First, the noise has been ignored in (4.174). Secondly, only the real part of the received signal is harvested for energy. The imaginary part has been discarded. Thirdly, instead of having a sum of signals from multiple users, (4.174) considers a sum of signals from multiple frequency bands and multiple antennas. Finally, instead of harvesting each signal and adding the harvested energy up, as in (4.163) and (4.164), (4.174) adds up the signals before harvesting them.

Using the received signal in (4.174), they aimed to maximize the output current at the energy harvester to give the following optimization problem as

$$\sum_{i \geq 2, ieven}^{n_0} k_i E\{y^i\}, \text{ with } \sum_{n=0}^{N-1} \sum_{m=1}^{M} |w_{n,m}|^2 < P \tag{4.175}$$

where n_0 is a constant that determines how much non-linearity of the energy harvester one can account for in the optimization, k_i is the parameter of the harvester, and other symbols are defined as before. When $n_0 = 2$, this model gives the linear harvester. In this case, it was shown in Clerckx and Bayguzina (2016) that the optimum waveforms are to transmit the full power P over the best channel among all frequencies and antennas. This agrees with our discussion before. If $n_0 > 2$, higher-order terms are included in the optimization and thus, the harvester is non-linear. In this case, it was reported in Clerckx and Bayguzina (2016) that one has to distribute the power over all different frequencies or antennas in order to maximize the output of the energy harvest. This again agrees with the observation from Chen et al. (2017d).

Both Chen et al. (2017d) and Clerckx and Bayguzina (2016) conclude that, if a linear harvester is used or the harvester operates in its linear region, the optimum strategy is to put the full power at the source with the best channel condition, and if a non-linear harvester is used or the harvester operates in its non-linear region, the optimum strategy is to distribute the power across all sources.

In another related work (Collado and Georgiadis 2014), the authors also investigated the effect of waveform on the conversion efficiency of the energy harvester. This is different from the results in Chen et al. (2017d) and Clerckx and Bayguzina (2016) in that here the conversion efficiency η is a function of the waveform, while it is a constant in most studies. The motivation of this work was that waveforms with higher peak-to-average-power ratio (PAPR) can activate the energy harvester with a lower threshold. The study in Collado and Georgiadis (2014) showed that the chaotic waveform has the highest conversion efficiency and thus, the largest harvested power, as it has the largest PAPR.

4.6 Other Issues and Techniques

In the previous sections, we have discussed energy harvesting detection, energy harvesting estimation, and energy harvesting waveform. These are the main design problems in the physical layer to solve the fundamental issues of any communications systems. In addition to these techniques, other advanced techniques may also be employed in the physical layer to solve one or two specific issues, such as security, spectral efficiency, and energy efficiency, to improve energy harvesting communications. Next, we will discuss some of these issues and techniques, including circuit power consumption, physical layer security, NOMA, and joint detection and estimation.

4.6.1 Circuit Power Consumption

Circuit power consumption is an important issue for energy harvesting communications. Many current energy harvesting communications systems are designed for low-power applications, such as wireless sensing and radio frequency identification (Sudevalayam and Kulkarni 2011). Consequently, the circuit power may not be negligible compared with the transmission power. In this subsection, we consider the case when the harvested power needs to cover both the circuit power and the transmission power for the remote device. Figure 4.27 shows a diagram of the circuit of the remote

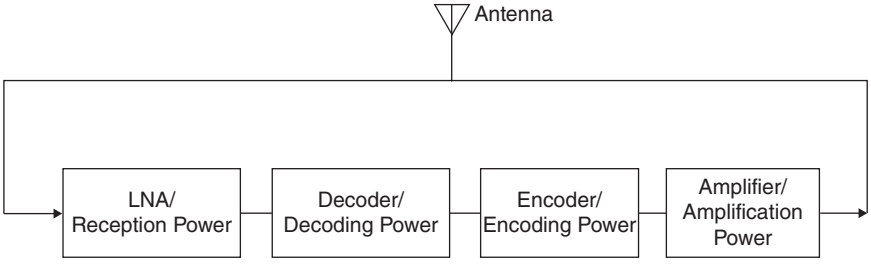

Figure 4.27 A diagram of the circuit of the remote device.

device considered in this book. The remote device needs to receive information from the access point and then responds to the information by sending its own data. Thus, four main parts of circuit power are considered: reception power; decoding power; encoding power; and amplification power.

Assume that the remote device uses a transmission power of P_x plus a circuit power of $P_c = P_{re} + P_{dc} + P_{ec} + P_{am}$, where P_{re} is the reception power, P_{dc} is the decoding power, P_{ec} is the encoding power, and P_{am} is the amplification power. It was reported in Bjornson et al. (2014) that, based on the central limit theorem, one has the amplification power and the reception power following Gaussian distributions with $\sqrt{P_{am}} \sim \mathcal{CN}(0, \delta_t^2 P_x)$ and $\sqrt{P_{re}} \sim \mathcal{CN}(0, \delta_r^2 P_r)$, respectively, where δ_r^2 and δ_t^2 are the parameters related to the receiver and transmitter structures, respectively, and P_r is the received signal power. Furthermore, one has $P_{dc} = F_{de} \cdot 2^{2B}$, $P_{ec} = F_{co} \cdot 2^{2B}$, where B is the bit resolution of the signal, and F_{de} and F_{co} are constants depending on the decoder and encoder structures, respectively (Chen et al. 2013).

Using all the above assumptions, the total power consumption including circuit power and transmission power can be written as

$$P_{tot} = P_x + \delta_t^2 P_x + F_{de} \cdot 2^{2B} + F_{co} \cdot 2^{2B} + \delta_r^2 P_r \tag{4.176}$$

where $P_{am} \approx E\{P_{am}\} = \delta_t^2 P_x$ and $P_{re} \approx E\{P_{re}\} = \delta_r^2 P_r$ have been used. Thus, if the power harvested from the access point is $P = \eta\beta^2 W$ as in (4.6), one has

$$\eta\beta^2 W = P_x + \delta_t^2 P_x + F_{de} \cdot 2^{2B} + F_{co} \cdot 2^{2B} + \delta_r^2 P_r. \tag{4.177}$$

This gives the new transmission power of the energy harvesting device as

$$P_x = \frac{1}{1 + \delta_t^2}[\eta\beta^2 W - F_{de} \cdot 2^{2B} - F_{co} \cdot 2^{2B} - \delta_r^2 P_r]. \tag{4.178}$$

This new transmission power can then be used in energy harvesting detection and energy harvesting estimation to design new detectors and estimators that consider the circuit power consumption. These designs will not be presented here as they are quite straightforward.

4.6.2 Physical Layer Security

Physical layer security has become increasingly important in recent communications systems. In fact, security is a fundamental problem in wireless communications due to the broadcast nature of the wireless medium. Traditional security measures often employ encryption algorithms at the upper layers. The most recent advance is to use the physical (PHY) layer security technique by exploiting the characteristics of the wireless fading channels for perfect secrecy (Liu and Trappe 2009). There are two unique aspects of the physical layer security technique in energy harvesting communications.

First, since the transmission power of an energy harvesting device is dynamic, the secrecy of the communications system becomes dynamic too. The secrecy rate is defined as the difference between the rate over the desired channel and the rate over the eavesdropping channel. Hence, the secrecy rate changes with the energy arrival process, and the average secrecy rate is often lower in such cases, similar to the BER analyzed before.

Secondly, for certain energy harvesting communications systems, such as the wireless powered systems to be discussed in Chapter 6, RF signals are employed to carry energy

as well as information, and the receiver receives the RF signals for both information decoding and energy harvesting. To do this, in practice, the transmitter has to increase its transmission power in order to facilitate energy harvesting at the receiver as extra energy is required at the receiver for harvesting. However, this also increases information leakage, as higher information energy is more susceptible to eavesdropping when there is an eavesdropper trying to intercept the information. Moreover, at the receiver, only a portion of the energy is used for information delivery, leading to a reduced rate. Thus, the security issue in the hybrid information and energy transmission will loom larger as a portion of the energy has to be used for power transfer.

Assume that Alice is an energy harvesting device and she sends information to Bob using the harvested energy. This communication is intercepted by an eavesdropper Eve. The received signal at Bob is given by

$$y_b = \sqrt{P_x} h_b s + n_b \tag{4.179}$$

where P_x is the transmitted power of Alice, h_b is the channel gain from Alice to Bob, s is the normalized transmitted symbol, and n_b is the AWGN with mean zero and variance $2\sigma^2$ at Bob. Similarly, the transmitted symbol will also be intercepted by Eve to have

$$y_e = \sqrt{P_x} h_e s + n_e \tag{4.180}$$

with an independent channel gain of h_e and noise of n_e. The secrecy rate is defined as

$$C_s = \max\left\{ \log_2\left(1 + \frac{P_x |h_b|^2}{2\sigma^2}\right) - \log_2\left(1 + \frac{P_x |h_e|^2}{2\sigma^2}\right), 0 \right\}. \tag{4.181}$$

In conventional communications, only the channel gains are random so that C_s needs to be averaged over the fading distributions to obtain the ergodic secrecy rate. In energy harvesting communications, both the channel gains and the transmission power can be random so that the averaging is performed over the channel gains as well as P_x. This is similar to the error rate analysis in Section 4.2.3. Also, the secrecy outage probability is defined as the probability that the rate in the desired channel is larger than that in the eavesdropping channel. Unlike the secrecy rate, energy harvesting does not change this secrecy outage probability.

On the other hand, if Alice is not an energy harvesting device but Bob is so that Alice needs to transmit her information as well as transfer a certain amount of energy to Bob so that Bob can harvest the energy for a response, the secrecy rate becomes

$$C_s = \max\left\{ \log_2\left[1 + \frac{(P_x + P_0)|h_b|^2}{2\sigma^2}\right] - \log_2\left[1 + \frac{(P_x + P_0)|h_e|^2}{2\sigma^2}\right], 0 \right\} \tag{4.182}$$

where P_x is the power used to guarantee the quality of information decoding at Bob, while P_0 is the extra power required by Bob for harvesting. Since the logarithm operation is non-linear, in general, the value of P_0 will lead to a different secrecy rate. This is the second effect of energy harvesting on the physical layer security.

There are many studies on other security issues in the literature. For example, in energy harvesting communications systems, some nodes are dedicated to energy harvesting while other nodes are dedicated to information decoding. Hence, the energy receivers could be potential eavesdroppers, or internal eavesdroppers (Pan et al. 2016). One may use interference alignment to nullify the signals for enhanced security (Zhao et al. 2017a). They are not discussed here.

4.6.3 Non-orthogonal Multiple Access

NOMA is one of the most recent advances in wireless communications. It aims to solve the spectral efficiency problem by using non-orthogonal channels in the power or code domain, compared with the conventional orthogonal multiple access (OMA) systems. In the following, we focus on the power domain NOMA.

In the power domain NOMA, signals for multiple users are superposed and transmitted over the same time slot, the same frequency, or the same code (Ding et al. 2017a). Multiple access is achieved by allocating different power coefficients to different users. Consider a two-user system as an example. The superposed signal is given by $a_1 s_1 + a_2 s_2$, where a_1 and a_2 are the power coefficients for user 1 and user 2 with $a_1^2 + a_2^2 = 1$, respectively, s_1 and s_2 are the transmitted signals for user 1 and user 2, respectively, with unit power. This signal is transmitted by the access point or base station. The received signal at user 1 is

$$y_1 = h_1 \sqrt{P_x}(a_1 s_1 + a_2 s_2) + n_1 \tag{4.183}$$

where h_1 is the channel gain from the base station to user 1 and n_1 is the AWGN with mean zero and variance $2\sigma^2$. The received signal at user 2 is

$$y_2 = h_2 \sqrt{P_x}(a_1 s_1 + a_2 s_2) + n_2 \tag{4.184}$$

where h_2 is the channel gain from the base station to user 2 and n_2 is the AWGN with mean zero and variance $2\sigma^2$.

The key idea of power domain NOMA is to allocate more power to the user with poorer channel condition. Thus, channel state information must be available. Assume that $|h_1| \leq |h_2|$. Then, $a_1 \geq a_2$. In this case, user 1 will decode its received signal y_1 directly so that its rate is

$$R_1 = \log_2 \left(1 + \frac{|h_1|^2 a_1^2}{|h_1|^2 a_2^2 + \frac{2\sigma^2}{P_x}} \right) \tag{4.185}$$

and user 2 will decode user 1's signal first and then use successive interference cancellation to decode its own signal so that its rate is

$$R_2 = \log_2 \left(1 + \frac{P_x |h_2|^2 a_2^2}{2\sigma^2} \right) \tag{4.186}$$

assuming perfect cancellation. The sum rate is therefore

$$R = \log_2 \left(1 + \frac{|h_1|^2 a_1^2}{|h_1|^2 a_2^2 + \frac{2\sigma^2}{P_x}} \right) + \log_2 \left(1 + \frac{P_x |h_2|^2 a_2^2}{2\sigma^2} \right). \tag{4.187}$$

It can be shown that this sum rate is larger than the sum rate in OMA in many cases. Thus, NOMA can achieve higher spectral efficiency. For more than two users, similar procedures can be applied, where the channel gains are first ordered and the power coefficients are assigned based on the order. Based on its power coefficient, each user either decodes its own signal directly by treating other users as interference or adopts successive interference cancellation before decoding.

For energy harvesting communications, if the access point or the base station harvest energy, the first effect of energy harvest is that the transmission power P_x may become

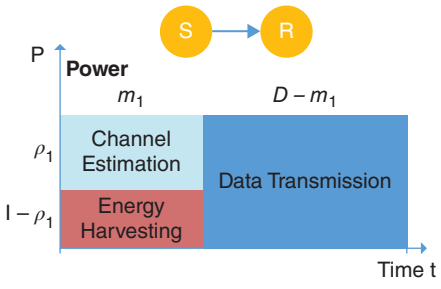

Figure 4.28 The data packet structure that splits pilots.

a random variable. Hence, the sum rate R is randomly varying, even if the channel gains are static. This is applicable to all energy harvesting communications systems where the access point harvests energy from the sun, wind or RF signals, etc. The energy arrival process will affect the power allocation within users and therefore the efficiency of NOMA. If the users harvest the RF signal from the base station, the second effect of energy harvesting is that this may change their order of decoding, depending on the portion of energy they harvest. Both effects can be examined by using a modified version of the sum rate. For example, the average sum rate can be obtained over P_x before the optimization of a_1 and a_2. Power splitting can be applied to y_1 and y_2 before deriving the rates.

Also, from the energy harvesting point of view, the non-orthogonal channels in NOMA actually provide more energy than the orthogonal channels in OMA, due to the extra multi-user interference. Interference degrades data performance but provides an extra source of energy.

4.6.4 Joint Detection and Estimation

The purpose of energy harvesting estimation is to provide the channel estimates for signal detection. Thus, signal detection and channel estimation need to be jointly considered with energy harvesting, similar to Section 4.4.2. In this case, there are three parts in the data packet that need to be balanced, as illustrated in Figure 4.25: energy harvesting; channel estimation; and data transmission. When the total resource is limited, there exists an optimum tradeoff between them. In this subsection, using a relaying system, we will discuss more cases of the tradeoff between data transmission, channel estimation and energy harvesting in a fixed data packet. The data packet structures studied in this subsection are shown in Figures 4.29, and 4.30. These data packets are for the source-to-relay link consisting of three parts: pilots for channel estimation; pilots for energy harvesting; and data for signal detection. For the relay-to-destination link, the data packet only has two parts, pilots for channel estimation and data for signal detection, as the destination does not need any energy harvesting.

Figure 4.28 shows data packet structure where the pilots for channel estimation have been split in power. In this structure, the source node only sends one group of pilots but each pilot is split in power for both energy harvesting and channel estimation. The data transmission happens in a time division manner. Figure 4.29 shows the data packet structure where the data symbols have been split in power. In this structure, the source sends one group of pilots for channel estimation, but the data symbols are split in power for both energy harvesting and data transmission. Figure 4.30 shows the data packet

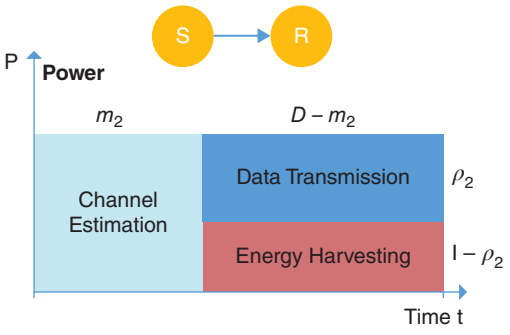

Figure 4.29 The data packet structure that splits data.

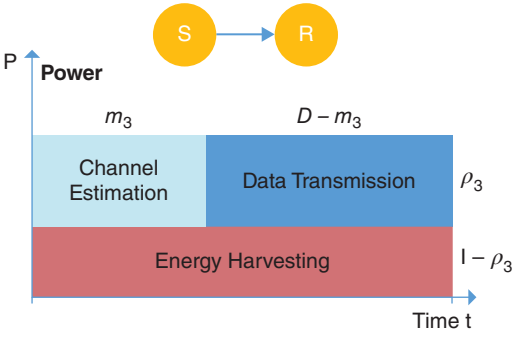

Figure 4.30 The data packet structure that splits both pilots and data.

structure where both pilots and data symbols have been split in power. In this structure, the source sends one group of pilots for channel estimation and one group of data symbols for information delivery. The energy is harvested by splitting all symbols in the data packet. This structure is similar to Figure 4.25.

The considered system is an amplify-and-forward relaying system with one source, one relay, and one destination, which means the signal is only amplified at the relay before being forwarded. There are two hops: the hop from source to relay (SR); and the hop from relay to destination (RD). The first hop assumes the structures in Figures 4.28–4.30, while the second hop only has one part for channel estimation and one part for data transmission without any energy harvesting. There is no direct link between source and destination due to obstacles. Time division is used in all the structures to achieve orthogonal channels. Therefore, the source first sends the data packet to the relay, and then the relay sends the data packet to the destination. Also, a total of D symbols are used in each structure for channel estimation, data transmission, and energy harvesting. Each symbol occupies a time duration of T seconds. All block fading channels are Rayleigh. All the values of m_1, m_2, and m_3 are integers and smaller than D. Also, $0 \leq \rho_1, \rho_2, \rho_3 \leq 1$.

In the first structure, there are three parts in the first hop: pilots for channel estimation and energy harvesting, and data symbols for information transmission. First, one has the received pilots at the relay for channel estimation as

$$y_r^{(i_1)} = \sqrt{\rho_1 P_{s1}} h_1 x^{(i_1)} + n_1^{(i_1)} \tag{4.188}$$

where $i_1 = 1, 2, \ldots, m_1$ represent the pilots in the data packet, ρ_1 is the power splitting factor, $0 < m_1 < D$ is an integer, P_{s1} is the transmitted power of the source, h_1 is the

fading gain in the SR channel and is complex Gaussian with mean zero and variance $2\alpha^2$, $x^{(i_1)} = 1$ is the transmitted pilot, and $n_1^{(i_1)}$ is the complex AWGN with mean zero and noise power $2\sigma^2$. The received pilots for energy harvesting can be expressed as

$$y_r^{(i_1)} = \sqrt{(1-\rho_1)P_{s1}}h_1 x^{(i_1)} + n_1^{(i_1)}. \tag{4.189}$$

In the same structure, the received data symbols are expressed as

$$y_r^{(j_1)} = \sqrt{P_{s1}}h_1 x^{(j_1)} + n_1^{(j_1)} \tag{4.190}$$

where $j_1 = m_1 + 1, \ldots, D$, and $x^{(j_1)}$ is the transmitted data symbol with unit power. Using (4.189), the harvested energy at the relay is derived as $E_{r1} = \eta P_{s1}|h_1|^2(1-\rho_1)m_1$, where η is the conversion efficiency of the energy harvester and we have assumed $T = 1$ for simplicity. The harvested energy will be used to transmit m_1 pilots to the destination for the channel estimation and $D - m_1$ data symbols from the source in the second hop in order to maintain the data rate. Thus, the transmission power of the relay is

$$P_{r1} = \frac{\eta P_{s1}|h_1|^2(1-\rho_1)m_1}{D}. \tag{4.191}$$

Also, using the signals in (4.188), we can get an estimate of h_1 as

$$\hat{h_1} = h_1 + \varepsilon_1 \tag{4.192}$$

where $\varepsilon_1 = \frac{\Sigma_{i_1=1}^{m_1} n_1^{(i_1)}}{m_1\sqrt{\rho_1 P_{s1}}}$ is the estimation error. Thus, one has $h_1 = \hat{h_1} - \varepsilon_1$.

The received signal in (4.190) will be amplified and forwarded to the destination by using the harvested energy. The amplification factor can be written as

$$\hat{a}_{1var}{}^2 = \frac{1}{P_{s1}|\hat{h_1}|^2 + 2\sigma^2} \tag{4.193}$$

where $\hat{h_1}$ is the estimated channel gain for the first hop between source node and relay node in (4.192).

In the second hop, the signal is transmitted from the relay to the destination. In addition to sending m_1 pilots to the destination for channel estimation, the relay also forwards the $D - m_1$ data symbols from the source to the destination. In this hop, the received pilots for channel estimation at the destination node can be written as

$$y_d^{(i_2)} = \sqrt{P_{r1}}g_1\hat{a}_{1var}x^{(i_2)} + n_2^{(i_2)} \tag{4.194}$$

where $i_2 = 1, 2, \ldots, m_1$, $x^{(i_2)} = 1$ is the pilot value, $n_2^{(i_2)}$ is the AWGN with zero-mean and variance $2\sigma^2$, $\hat{a}_{1var}$ is the amplification factor, P_{r1} is the relay transmission power given in (4.191), and g_1 is the fading channel coefficient of the RD link and is a complex Gaussian random variable with mean zero and variance $2\alpha^2$.

Also, the received signals of the data symbols at the destination are given by

$$y_d^{(j_2)} = \sqrt{P_{r1}}g_1\hat{a}_{1var}(\sqrt{P_{s1}}h_1 x^{(j_1)} + n_1^{(j_1)}) + n_2^{(j_2)} \tag{4.195}$$

where $n_2^{(j_2)}$ is the AWGN at the destination node with zero mean and variance $2\sigma^2$.

By using the received signals in (4.194), the channel gain of the RD link can be estimated as

$$\hat{g_1} = \frac{\sqrt{P_{r1}}}{\sqrt{\hat{P_{r1}}}}g_1 + \varepsilon_2 \tag{4.196}$$

where $\varepsilon_2 = \frac{\sum_{i_2=1}^{m_1} n_2^{(i_2)}}{m_1 \hat{a}_{1var}\sqrt{P_{r1}}}$ and $\hat{P_{r1}} = \frac{\eta P_{s1}|\hat{h_1}|^2(1-\rho_1)m_1}{D}$.

By using the channel estimates in (4.195), the received signal at the destination can be rewritten as

$$\begin{aligned} y_d^{(j_2)} &= \sqrt{\hat{P_{r1}}}\hat{g_1}\hat{a}_{1var}\sqrt{P_{s1}}\hat{h_1}x^{(j_1)} \\ &\quad - \sqrt{\hat{P_{r1}}}\hat{g_1}\hat{a}_{1var}\sqrt{P_{s1}}\varepsilon_1 x^{(j_1)} \\ &\quad + \sqrt{\hat{P_{r1}}}\hat{g_1}\hat{a}_{1var}n_1^{(j_1)} \\ &\quad - \sqrt{\hat{P_{r1}}}\sqrt{P_{s1}}\hat{h_1}\hat{a}_{1var}\varepsilon_2 x^{(j_1)} \\ &\quad + \sqrt{\hat{P_{r1}}}\sqrt{P_{s1}}\hat{a}_{1var}\varepsilon_1\varepsilon_2 x^{(j_1)} \\ &\quad - \sqrt{\hat{P_{r1}}}\varepsilon_2\hat{a}_{1var}n_1^{(j_1)} + n_2^{(j_2)}. \end{aligned} \tag{4.197}$$

From the above, the end-to-end SNR expression can be derived as

$$\gamma_{1end} = \frac{P_{s1}|\hat{g_1}|^2|\hat{h_1}|^2}{\upsilon_1} \tag{4.198}$$

where $\upsilon_1 = P_{s1}|\hat{g_1}|^2\varepsilon_{1var} + 2\sigma^2|\hat{g_1}|^2 + P_{s1}\varepsilon_{2var}|\hat{h_1}|^2 + P_{s1}\varepsilon_{1var}\varepsilon_{2var} + 2\sigma^2\varepsilon_{2var} + \frac{2\sigma^2}{\hat{P_{r1}}\hat{a}_{1var}{}^2}$ and $E[|\varepsilon|_1^2] = \varepsilon_{1var}$, $E[|\varepsilon|_2^2] = \varepsilon_{2var}$.

To derive the cumulative distribution function of the end-to-end SNR, we first calculate $Var(\varepsilon_1)$ and $Var(\varepsilon_2)$. One has already had

$$\varepsilon_1 = \frac{\sum_{i_1=1}^{m_1} n_1^{i_1}}{m_1\sqrt{\rho_1 P_{s1}}}. \tag{4.199}$$

It has a mean of zero. Also, its variance is

$$Var(\varepsilon_1) = E\{|\varepsilon_1|^2\} = \frac{2\sigma^2}{m_1\rho_1 P_{s1}}. \tag{4.200}$$

Similarly, the variance of ε_2 can be calculated as

$$Var(\varepsilon_2) = \frac{2\sigma^2 D(P_{s1}|\hat{h_1}|^2 + 2\sigma^2)}{[\eta P_{s1}|\hat{h_1}|^2(1-\rho_1)m_1]m_1}. \tag{4.201}$$

These two equations can be used in the end-to-end SNR.

Further, $|\hat{h_1}|^2$ is an exponential random variable with scale parameter

$$\lambda_1 = \frac{1}{2\alpha^2 + \frac{2\sigma^2}{m_1\rho_1 P_{s1}}}. \tag{4.202}$$

The probability density function (PDF) of $|\hat{h_1}|^2$ can be written as

$$f_{|\hat{h_1}|^2}(x) = \lambda_1 e^{-\lambda_1 x}. \tag{4.203}$$

Its CDF is

$$F_{|\hat{h_1}|^2}(x) = 1 - e^{-\lambda_1 x}. \tag{4.204}$$

Similarly, let $\lambda_2 = \frac{1}{\frac{4\alpha^4}{2\alpha^2+\frac{|2\sigma^2|}{m_1\rho_1 P_{s1}}} + \frac{|2\sigma^2||m_2+D-m_1|\rho_1}{|m_2|\eta|1-\rho_1|m_1}}$. Its PDF can be approximated as

$$f_{|\hat{g}_1|^2}(x) = \lambda_2 e^{-\lambda_2 x} \tag{4.205}$$

and its CDF can be approximated as

$$F_{|\hat{g}_1|^2}(x) = 1 - e^{-\lambda_2 x}. \tag{4.206}$$

By using these expressions, the CDF of γ_{1end} can be derived as

$$F_{\gamma_{1end}}(x) = P_{1r}\{\gamma_{1end} < x\} = I_{11} + I_{12} \tag{4.207}$$

with

$$I_{11} = 1 - e^{-\frac{\frac{2\sigma^2 x}{m_1\rho_1 P_{s1}} + \frac{2\sigma^2 x}{P_{s1}}}{2\alpha^2 + |\frac{2\sigma^2}{m_1\rho_1 P_{s1}}|}} \tag{4.208}$$

and

$$\begin{aligned} I_{12} = & \frac{1}{P_{s1}\left(2\alpha^2 + \frac{2\sigma^2}{m_1\rho_1 P_{s1}}\right)} e^{-\frac{2\sigma^2 x + 2\sigma^2 x m_1\rho_1}{2\alpha^2 m_1\rho_1 P_{s1} + 2\sigma^2}} \frac{2\alpha^2 m_1\rho_1 P_{s1} + 2\sigma^2}{m_1\rho_1} \\ & - \frac{1}{\left(2\alpha^2 + \frac{2\sigma^2}{m_1\rho_1 P_{s1}}\right)} \\ & \cdot e^{-\frac{\lambda_2 m_1 x 2\sigma^2\rho_1(D)}{\eta\rho_1 m_1(1-\rho_1)m_1{}^2 P_{s1} y} - \frac{2\sigma^2 x + 2\sigma^2 x m_2}{2\alpha^2 m_1\rho_1 P_{s1} + 2\sigma^2}} \\ & \cdot \frac{2}{P_{s1}} \left(\frac{z_1(x)}{(\eta m_1(1-\rho_p)m_1{}^2)m_1}\right)^{\frac{1}{2}} K_1\left(2\sqrt{\frac{z_2(x)}{w_4}}\right) \end{aligned} \tag{4.209}$$

where $w_4 = (\eta m_1(1-\rho_1)m_1{}^2)(2\alpha^2 m_1\rho_1 P_{s1} + 2\sigma^2)$, $z_1(x) = (\frac{1}{\frac{4\alpha^4}{2\alpha^2+\frac{2\sigma^2}{m_1\rho_1 P_{s1}}} + \frac{2\sigma^2 D\rho_1}{m_1\eta|1-\rho_1|m_1}})$ $(4\sigma^4 xD +$ $4\sigma^4 m_1\rho_1 xD + 2\sigma^2 x m_1 m_1\rho_1 D + 2\sigma^2 m_1 xD * \frac{2\sigma^2 x\rho_1}{m_1\rho_1} + 2\sigma^2 x\rho_1)$ $(2\alpha^2 m_1\rho_1 P_{s1} + 2\sigma^2)$ and $z_2(x) = (\frac{1}{\frac{4\alpha^4}{2\alpha^2+\frac{2\sigma^2}{m_1\rho_1 P_{s1}}} + \frac{2\sigma^2 D\rho_1}{m_1\eta|1-\rho_1|m_1}})$ $(4\sigma^4 xD + 4\sigma^4 m_1\rho_1 xD$ $+2\sigma^2 x m_1 m_1\rho_1 D + 2\sigma^2 m_1 xD *$ $\frac{2\sigma^2 x\rho_1}{m_1\rho_1} + 2\sigma^2 x\rho_1)m_1$.

The outage probability can then be derived as

$$P_0(\gamma_{01}) = F_{\gamma_{1end}}(\gamma_{01}). \tag{4.210}$$

Moreover, the BER can be calculated as

$$BER_1 = \frac{1}{2}\int_0^\infty \frac{e^{-x}}{\sqrt{x * \pi}} F_{\gamma_{1end}}(x)dx. \tag{4.211}$$

where erfc(x) is the complementary error function. The structures in Figures 4.29 and 4.30 can be analyzed in a similar way. The analysis is ignored here for brevity.

Figures 4.31–4.34 show the performances of the first structure in Figure 4.28 for different parameters. One can see that there are optimum values of m and optimum values of ρ_1 in all the cases considered. The SNRs will change the locations of the optimum

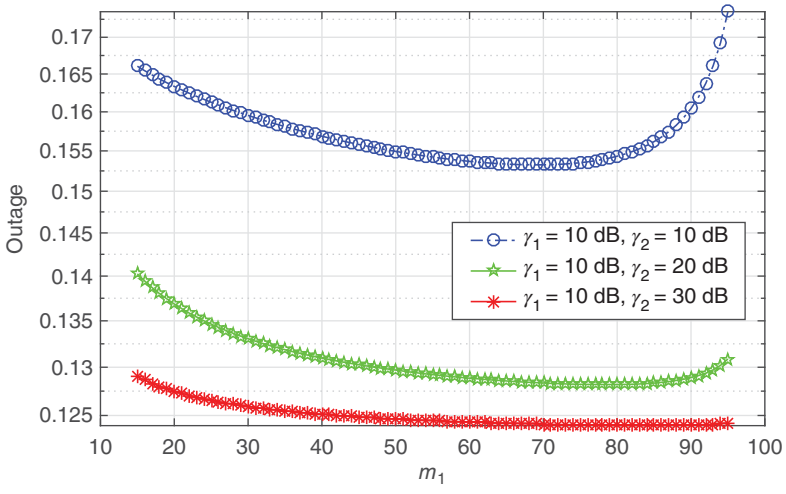

Figure 4.31 Outage versus m_1.

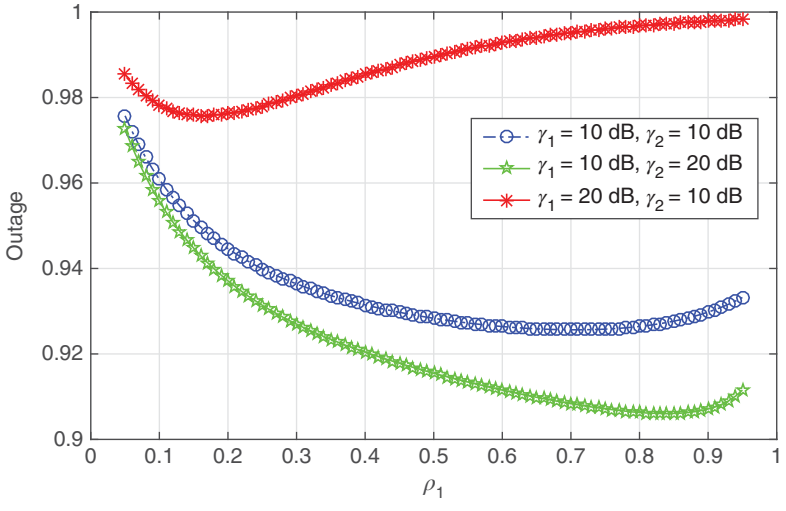

Figure 4.32 Outage versus ρ_1.

values. This is expected, as a larger value of m_1 leads to more pilots for a more accurate channel estimate but this reduces the number of data symbols that can be transmitted. Similarly, a larger value of ρ_1 allows more energy for channel estimation for a more accurate channel estimate but it also reduces the amount of energy harvested and hence a smaller transmission power for the relay, leading to poorer performances. Similar trade-offs exist for the other two data packet structures. Thus, for energy harvesting detection and estimation, it is important to allocate the appropriate amount of energy for channel estimation, energy harvesting and data transmission to achieve the optimum performances.

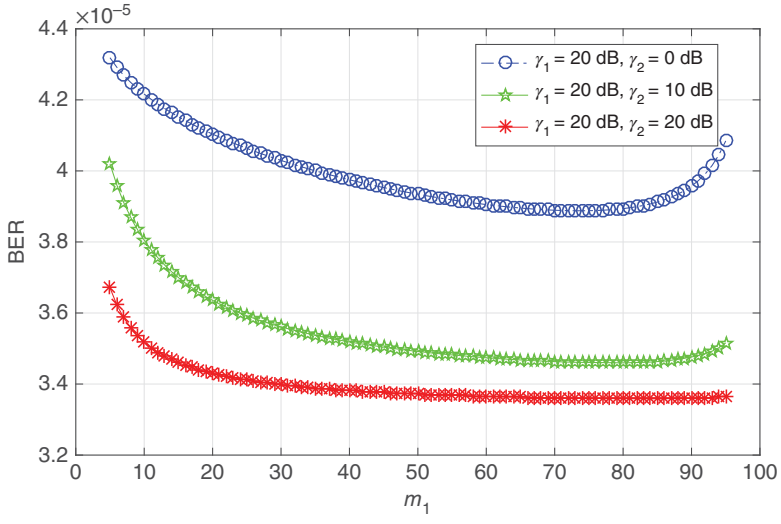

Figure 4.33 BER versus m_1.

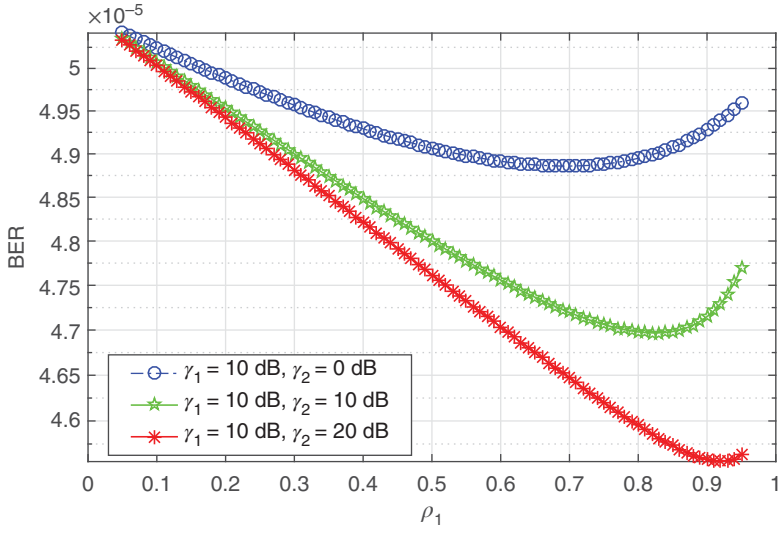

Figure 4.34 BER versus ρ_1.

4.7 Summary

In this chapter, we have discussed several main physical layer techniques in energy harvesting communications systems.

First, the effect of energy harvesting on the physical layer techniques in conventional communications systems has been examined. The examination has shown that, if the fixed-power transmission strategy is employed so that the energy harvesting device accumulates energy to transmit signals at a fixed power, there is an optimum number

of time slots or harvesting time the device can choose to balance the requirement for transmission power and transmission delay. If the variable-power transmission strategy is used so that the energy harvesting device transmits as soon as the energy is harvested, the BER and rate performances will be degraded due to the random variation in the transmission power.

Secondly, new signal detectors, new channel estimators and new transmission waveforms for energy harvesting have been designed. For signal detection, the random transmission power must be considered in the detector design when it is unknown. For channel estimation, energy harvesting reduces the resources used for channel estimation and hence, an optimum tradeoff between energy harvesting, channel estimation and data transmission exists, when the total amount of resources is fixed. For waveform designs, if a linear energy harvester is applied or a single sum signal is used, the optimum strategy is always to put all the transmission power at the source with the best channel condition, while if a non-linear energy harvester is applied for a sum of harvested energy, the best strategy is to allocate different amplitudes to different sources, while the phase of the waveform can be arbitrary.

Finally, several other important physical layer issues have also been discussed briefly. For the circuit power, if it is considered in the design, it normally degrades the rate performance, as part of the harvested energy needs to be used for circuit power consumption. For the physical layer security, the random variation in the transmission power can affect the secrecy rate, while for NOMA, the decoding order and the power allocation of different users can be changed due to energy harvesting. For joint detection and estimation, the balance between channel estimation, energy harvesting and data transmission within a fixed data packet is required to achieve optimum performances.

To summarize, the physical layer techniques in energy harvesting communications have two main characteristics. The first characteristic is that the transmission power or the transmission time of an energy harvesting device can be random, due to the random energy arrival process. The second characteristic is that the resources for other functions in the physical layer can be reduced, due to the addition of the energy harvesting function, if the total resource is limited. In the next chapter, we will discuss the upper layer issues in energy harvesting wireless communications systems.